

Hadamard Representations: Augmenting Hyperbolic Tangents in RL

Jacob E. Kooi¹ Mark Hoogendoorn¹ Vincent François-Lavet¹

Abstract

Activation functions are one of the key components of a deep neural network. The most commonly used activation functions can be classed into the category of continuously differentiable (e.g. tanh) and piece-wise linear functions (e.g. ReLU), both having their own strengths and drawbacks with respect to downstream performance and representation capacity through learning. In reinforcement learning, the performance of continuously differentiable activations often falls short as compared to piece-wise linear functions. We show that the dying neuron problem in RL is not exclusive to ReLUs and actually leads to additional problems in the case of continuously differentiable activations such as tanh. To alleviate the dying neuron problem with these activations, we propose a Hadamard representation that unlocks the advantages of continuously differentiable activations. Using DQN, PPO and PQN in the Atari domain, we show faster learning, a reduction in dead neurons and increased effective rank.

1. Introduction

The Rectified Linear Unit (ReLU) (Fukushima, 1969; Nair & Hinton, 2010) and its variants (Xu et al., 2015; Klambauer et al., 2017) have emerged as the most widely used and generally best-performing activation functions up until this day (Jarrett et al., 2009; Goodfellow et al., 2016). The strength of the ReLU activation lies in its ability to naturally avoid vanishing gradients when used in deeper networks, in contrast to the continuously differentiable activation functions, such as the sigmoid and the hyperbolic tangent (Glorot & Bengio, 2010).

A common drawback of using the ReLU activation is its limited expressivity in the context of shallow networks (see Fig. 2), as well as the phenomenon known as the dying

¹Department of Computer Science, Vrije Universiteit Amsterdam. Jacob E. Kooi <j.e.kooi@vu.nl>, Mark Hoogendoorn <m.hoogendoorn@vu.nl>, Vincent François-Lavet <vincent.francoislavet@vu.nl>.

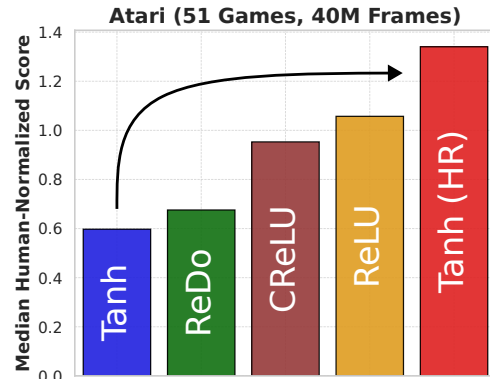


Figure 1: Median Human-Normalized performance training PQN in the Atari domain where the activation function of the hidden layers is changed. In PQN, all activations are already layer-normalized. A massive performance discrepancy in performance can be observed when selecting different activation functions. Notably, in Atari, the application of a Hadamard representation with hyperbolic tangent leads to over 100% performance gains. The Hadamard representation is not suitable for the ReLU activation, as it amplifies dying neurons by taking the product of sparse activations.

ReLU problem (He et al., 2015; Lu et al., 2019). As training progresses, the number of dying ReLUs tend to increase, resulting in a dying network and loss of network capacity (Dubey et al., 2022).

In reinforcement learning (RL) (Sutton & Barto, 2018), the dying neuron phenomenon is much more prevalent than in supervised learning due to the use of non-stationary targets (Sokar et al., 2023). However, even though training results in a large number of dying ReLUs (Gulcehre et al., 2022; Sokar et al., 2023), the ReLU function still remains the most popular activation for performance reasons (Henderson et al., 2018). Similar to supervised learning (Teney et al., 2024), continuously differentiable activation functions such as the hyperbolic tangent are therefore not favored in RL (see Fig. 1). However, one might argue that their symmetrical, bounded shape and smooth gradient landscape offer optimization advantages that the ReLU lacks. Recent findings also indicate that a hidden layer activated by a hyperbolic tangent displays a high effective rank and thus a

high layer expressivity (Kumar et al., 2021; Gulcehre et al., 2022). Despite being a theoretically sound candidate, its lack of success in RL has not been thoroughly investigated.

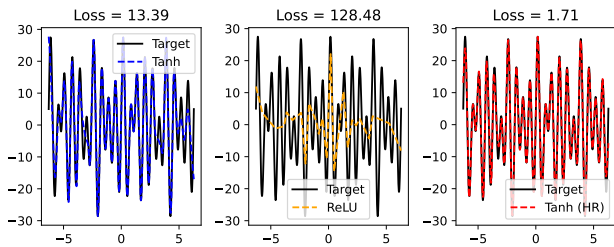


Figure 2: A regression of three shallow neural network architectures on a random complex sinusoidal function ($y = 10 * torch.sin(7 * x) + 15 * torch.sin(10 * x) + 5 * torch.cos(5 * x)$). The Tanh (HR) network emerges as the strongest function approximator, even while having less trainable parameters (501 vs 601 for Tanh & ReLU). To make a fair comparison, the Tanh and ReLU networks have one single hidden layer of size 200, while the Tanh (HR) network has a hidden layer of size 100. For the Tanh (HR) network however, we use two parallel linear layers preceding the hidden layer in order to be able to use the single hidden layer as the Hadamard product of two activations (see Section 4). For experiments comparing deeper networks, we refer the reader to Appendix C.1.

This paper provides insights into the hyperbolic tangent’s suboptimality, revealing that RL gradients lead to bias-inducing dying neurons and under-utilization of the full network capacity. Based on these insights, we mitigate said effects by augmenting the original hidden layer architecture. Specifically, we provide an alternative to the conventional parameterization of these layers. Our contributions can be summarized as follows:

- We show that, in reinforcement learning, dying hyperbolic tangents are a phenomenon of a similar scale as the dying ReLU problem, and argue how they inherently have a more profound effect on performance.
- A Hadamard representation (HR) is proposed, defining a hidden layer as the Hadamard product of two separate, individually parameterized activation vectors.
- We empirically show that, without hyperparameter tuning or the use of auxiliary losses, Hadamard representations yields notable performance gains in multiple algorithms in the Atari domain, and reveal how it decreases dying neurons and increases the internal representations’ effective rank.

2. Related Work

This section provides related work from the perspective of: (i) the loss of capacity through learning neural networks and (ii) the effect of different network architectures in RL.

Network Capacity in RL. Liu et al. (2019) investigated the need for sparse representations in the continuous control domain. Gulcehre et al. (2022) analyzed network expressiveness in RL by measuring the effective rank (Kumar et al., 2021) of the representation, and found that hyperbolic tangent representations generally maintain high rank while not suffering strongly from rank decay as training continues. Related work used normalization techniques and action penalization to counteract high variance in pixel-based robotic control (Bjorck et al., 2022). Other work by Lyle et al. (2022) investigated capacity loss in RL and similarly found that, as training progresses, the inherent network capacity of RL algorithms decays. Further research by Nikishin et al. (2022) used network resets to counteract the primacy bias and (Sokar et al., 2023) evaluated and mitigated the dying ReLU phenomenon in DQN, both operating in the sample efficiency setting. Nikishin et al. (2023) further studied plasticity injection for long-term training and Delfosse et al. (2024) applied rational activations (Molina et al., 2019) in RL to increase plasticity. Concurrent work by Dohare et al. (2024) used continual back-propagation to further alleviate plasticity loss. In another related direction, recent work has investigated network sparsity in RL, showing that a large part of network capacity might be unnecessary when training reinforcement learning (Arnob et al., 2021; Graesser et al., 2022; Sokar et al., 2022; Tan et al., 2023; Obando-Ceron et al., 2024). This provides insights into why a ReLU can achieve strong performance despite resulting in a significant number of dead neurons.

Network Architecture in RL The origin of network optimization problems with hyperbolic tangents and sigmoids were empirically investigated by Glorot & Bengio (2010), where, according to the authors, a lot of mystery still surrounds the subject. Work by (Srivastava et al., 2015) in supervised learning first looked at the idea of using products of hidden layers together with a ‘gate’ that determined the amount of information flow (Hochreiter & Schmidhuber, 1997). Using these ideas, the Resnet was invented (He et al., 2016) and also showed strong performance in combination with RL (Espeholt et al., 2018). Further work by Henderson et al. (2018) showed differences in RL performances over different network architectures and nonlinear activations. Work by Abbas et al. (2023) successfully applied ReLU concatenation (Shang et al., 2016) to improve continual learning while keeping a similar performance when training from scratch. Finally, recent work by Grooten et al. (2024) investigated raw pixel masking for distractions in RL using a parallel CNN input layer.

3. Preliminaries

We consider an agent acting within its environment as a discrete Markov Decision Process (MDP) defined as a tuple $(\mathcal{S}, \mathcal{A}, T, R, \gamma)$. \mathcal{S} is the state space, \mathcal{A} is the action space, $T : \mathcal{S} \times \mathcal{A} \rightarrow \mathbb{P}(\mathcal{S})$ is the environment’s transition function, $R : \mathcal{S} \times \mathcal{A} \rightarrow \mathcal{R}$ is the environment’s reward function and $\gamma \in [0, 1)$ is the discount factor. A replay buffer B is used to store visited states $s_t \in \mathcal{S}$ that were followed by actions $a_t \in \mathcal{A}$ and resulted in the rewards $r_t \in \mathcal{R}$ and the next states s_{t+1} . One entry in B contains a tuple of past experience (s_t, a_t, r_t, s_{t+1}) . The agent’s goal is to learn a policy $\pi : \mathcal{S} \rightarrow \mathcal{A}$ that maximizes the expectation of the discounted return $V^\pi(s) = \mathbb{E}_\tau[\sum_{t=0}^{\infty} \gamma^t R(s_t, a_t) \mid s_t = s]$, where τ is a trajectory following the policy π .

4. Augmenting Hyperbolic Tangents

Continuously differentiable activations such as the hyperbolic tangent (\tanh) and the sigmoid (σ) activations are fundamentally different than the ReLU or its piece-wise linear descendants, which are non-symmetric and have a large part of the input space mapped to zero (leading to sparsity). The hyperbolic tangent and the sigmoid output values in the ranges $[-1, 1]$ and $[0, 1]$, respectively. These functions are defined as $\tanh(x) = \frac{e^x - e^{-x}}{e^x + e^{-x}}$ and $\sigma(x) = \frac{1}{1 + e^{-x}}$.

Both functions have the advantage of being differentiable everywhere, as well as being bounded. Furthermore, the sigmoid is well suited for output probabilities, while the tanh is convenient when requiring a zero-centered symmetrical output. However, both functions exhibit the vanishing gradient problem for saturating activations (Glorot & Bengio, 2010; Goodfellow et al., 2016).

Dying Hyperbolic Tangents

Although the literature has focused on the dying ReLU problem (He et al., 2015; Lu et al., 2019; Gulcehre et al., 2022; Sokar et al., 2023), we find that hidden layers activated by hyperbolic tangents similarly show strong dying neuron behavior, particularly in the RL context with the moving target from the Bellman iterations. When using any activation function in a deep neural network, a single neuron $\alpha_i, i \in \mathbb{R}^w$, with w the layer dimension, is saturated or dying if:

$$\alpha_i \approx \Omega, \forall s_t \in B \quad (1)$$

Where Ω represents the saturation value and s_t is an observation in buffer B . In practice, a mini-batch of observations is evaluated instead of the whole dataset in B . For the hyperbolic tangent, given that it is an asymptotic function near its saturation point, an approximate equality is considered ($|\alpha_i| \neq 1, \forall s_t \in B$). To approximate the condition

given in Eq. 1, the amount of dying hyperbolic tangents is calculated by using a kernel density estimation (KDE) (Silverman, 1986) on the activations $\alpha_i, i \in \mathbb{R}^w$ of each individual neuron in the activation layer. In order to visualize activations in a hidden layer, a fixed subset of the KDE’s of the neurons α_i is taken. A clear visualization of dying hyperbolic tangents during training in the Atari Breakout environment can be seen by analyzing sixteen individual neuron KDE’s in Fig. 3. Massive KDE spikes at either 1 or -1 represent the absence of neuron variance over a batch of observations, meaning that the neuron has lost its value to propagate useful information. More details on the KDE calculation and dying neuron classification can be found in Appendix B.

Hyperbolic Tangents turn Weights into Biases

When dying neurons occur in ReLU-activated layers, it basically prunes these neurons and the associated weights to the next layer. However, in hyperbolic tangent activated layers, dying neurons lead to an unintended phenomenon where weights associated with dead neurons effectively become biases.

Theorem 4.1. *When any set of neurons α_i^j in a hidden layer z^j collapses into nonzero values, the output to the next layer effectively changes from $(A^j z^j + B^j)$ to $(A_{-*}^j z_{i-*}^j + B^{j+1} + A_*^j z_{i*}^j)$, where $A_{-*}^j z_{i-*}^j$ represent the active neurons multiplied by their corresponding forward-connected weights and $A_*^j z_{i*}^j = B_*^{j+1}$ represent the dead neurons multiplied by their corresponding weights, resulting in the hidden bias B_*^{j+1} .*

Proof. Let us consider a set of neurons α_i^j and forward connected weights $w_{\alpha_i}^j$ in the hidden layer z^j . The influence of these neurons on the next hidden layer z^{j+1} is calculated as:

$$z^{j+1} = \sum_i \alpha_i^j w_{\alpha_i}^j + B^{j+1}. \quad (2)$$

If the set of neurons dies and collapses into 0 ($\alpha_i^j = 0, \forall s \in \mathcal{S}$), which occurs when using ReLU activations, the influence on the next layer becomes 0, representing basic pruning:

$$\sum_i 0 \cdot \bar{w}_{\alpha_i}^j = 0, \quad \forall s \in \mathcal{S}. \quad (3)$$

Where $\bar{w}_{\alpha_i}^j$ is the set of weights connected to the dying neurons. However, for a hyperbolic tangent activation, if the set of neurons saturate into either -1 or 1 ($\alpha_i^j = \{1, -1\}, \forall s \in \mathcal{S}$), the output is

$$\sum_i \{1, -1\} \cdot \bar{w}_{\alpha_i}^j = B_*^{j+1}, \quad \forall s \in \mathcal{S}. \quad (4)$$

As a result, the weight vector $\bar{w}_{\alpha_i}^j$ corresponding to the dying activations only influences a bias B_*^{j+1} on the next

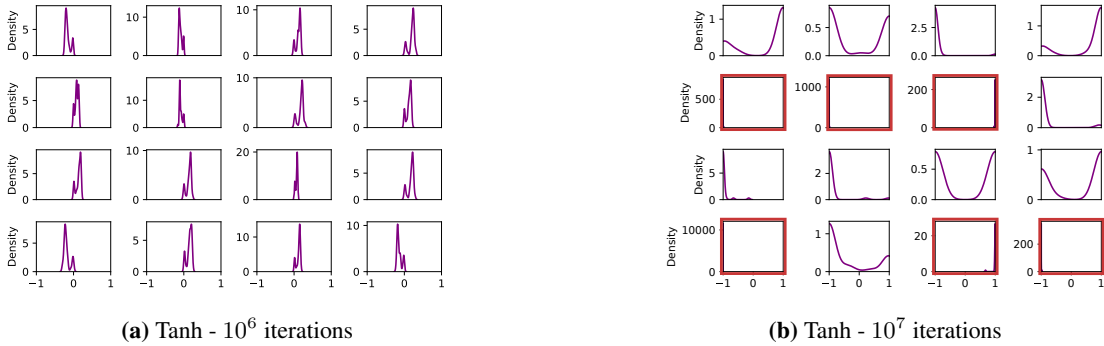


Figure 3: Kernel Density Estimations (KDE) over a subset of 16 neurons in the compressed representation z_t after training DQN (Mnih et al., 2015) in the Breakout environment using a hyperbolic tangent activation for z_t . Each neuron represents one dimension of the representation $z_t \in \mathbb{R}^{512}$. Red outlines represent dying neurons, where a near infinite sized density spike occurs at either 1 or -1.

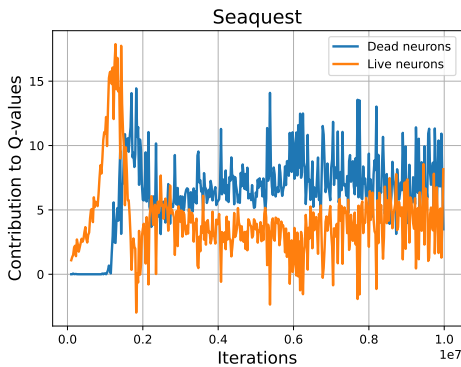


Figure 4: 10M iterations (40M frames) training DQN with a hyperbolic tangent activation in the Seaquest environment. The average contribution to the Q-values of the live and dead neurons in the final hidden layer is observed. If a neuron dies, it retains the same value for any input observation, but a multiplication of the nonzero saturation value with its outgoing weights implements a substantial ‘hidden’ bias on the Q-values.

layer. Note that the bias B_*^{j+1} is constant for any input observation. \square

This emergent bias can hinder the optimization process by introducing unintended fixed contributions to a networks’ hidden layers or output layer, reducing the flexibility of the network’s representations and potentially reducing its performance in RL or supervised learning. For example, in Atari’s Seaquest environment, we can see that this bias is substantial and nonzero (see Fig. 4).

Hadamard Representations (HR)

As Fig. 3 indicates that the activation of z_t with a hyperbolic tangent leads to saturation and dying neurons, an augmen-

tation of the representation architecture is proposed. In the conventional encoder setting, a network’s hidden layer can be defined as $z^{enc}(x) = f(A_1x + B_1)$, with A_i and B_i representing weight and bias parameters, the function $f(\cdot)$ representing a nonlinear activation function while x is the set of activations from the previous layer. In order to reduce the information dependence on a single set of neurons, we propose using a Hadamard representation that augments the original representation with a parallel representation layer z^* . This can be interpreted as using a single highway layer with a closed carry gate (Srivastava et al., 2015), or as an augmented version of the Gated Linear Unit (GLU) (Dauphin et al., 2017). The final representation is defined as a Hadamard product between the aforementioned activations $z(x) = z^{enc}(x) \cdot z^*(x)$, where $z^*(x) = f(A_2x + B_2)$. A visualization of the proposed architecture can be found in Fig. 5.

Preventing Dying Neurons

Our key hypothesis is that the Hadamard representation can prevent saturation, hence alleviating vanishing gradients and dying neurons (See Eq. 1). To support our hypothesis, we investigate the derivative of a product of two functions. For the product of two arbitrary functions $g(x) \cdot h(x)$, the derivative is defined as $g'(x)h(x) + g(x)h'(x)$. In the context of using a sigmoid activation function for $f(x)$, the derivative of $z(x)$ becomes:

$$z'(x) = \frac{A_1\sigma(A_1x + B_1)(1 - \sigma(A_1x + B_1))\sigma(A_2x + B_2) + A_2\sigma(A_1x + B_1)\sigma(A_2x + B_2)(1 - \sigma(A_2x + B_2))}{\sigma(A_1x + B_1)\sigma(A_2x + B_2)}$$

If a neuron from $f(A_1x + B_1) = 0 \forall x$, the gradient of the product becomes 0 while if a positive saturation is experienced i.e. $f(A_1x + B_1) = 1 \forall x$, $z'(x)$ can remain nonzero. For a product of two hyperbolic tangent functions,

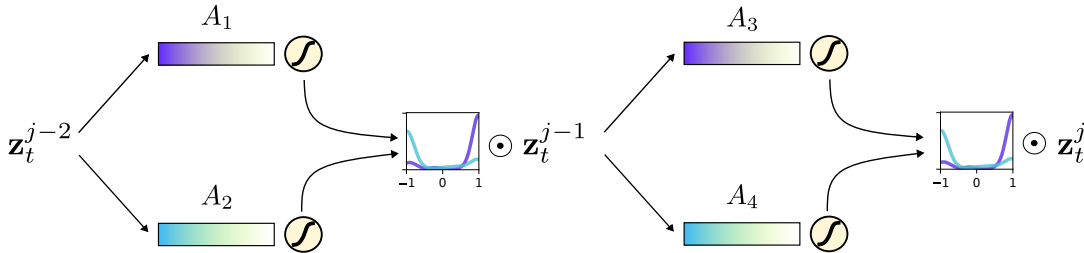


Figure 5: A visualisation of the Hadamard representation. Horizontal bars represent weight vectors and z_t represents a hidden layer. Between each hidden layer, two parallel independently parameterized activation layers are formed, where the Hadamard product of the two activation layers represents the actual propagated hidden layer.

the derivative is defined as:

$$z'(x) = \frac{A_1 \operatorname{sech}^2(A_1x + B_1) \tanh(A_2x + B_2)}{+ A_2 \operatorname{sech}^2(A_2x + B_2) \tanh(A_1x + B_1)}.$$

In this context, sech^2 is the derivative of the hyperbolic tangent function. Unlike the sigmoid, the hyperbolic tangent saturates to nonzero values, ensuring that if and only if both parts are saturated, product saturation occurs. Thus, when $g(x)$ saturates, $h(x)$ still keeps a non-trivial gradient in the product, providing a mechanism to avoid vanishing gradients. We visualize the kernel densities during training with a Hadamard representation in Fig. 6. The individual representations before taking the Hadamard product can be found in Appendix B.

Taking a more formal approximation of neuron collapse, we start by defining the probability of a single neuron saturating as \mathbf{p} . Furthermore, in the case of a sigmoid or hyperbolic tangent, we assume symmetric saturation probabilities to both ends, defining the probability of a neuron saturating to one end of the spectrum as $0.5\mathbf{p}$. Lastly, we make an independence assumption between two individual neurons. Under these assumptions, we show that interpreting a neuron as the product of two individual neurons can change saturation probabilities depending on the neuron’s activation function.

Hyperbolic Tangent: In the case of the hyperbolic tangent, product saturation only occurs if strictly both neurons are saturated. This results in a probability of $\mathbf{p} \cdot \mathbf{p} = \mathbf{p}^2$. Taking a product of hyperbolic tangent activated neurons thus reduces the neuron saturation probability from \mathbf{p} to \mathbf{p}^2 .

Sigmoid: For the sigmoid function, product saturation occurs in two scenarios: Either one of the neurons is saturated towards zero or both neurons are saturated towards 1. The probability that a single neuron does not saturate towards zero is $(1 - 0.5\mathbf{p})$, and subsequently the probability that neither neuron saturates towards zero is $(1 - 0.5\mathbf{p})^2$. The

probability that at least one of the two neurons saturates to zero is therefore $1 - (1 - 0.5\mathbf{p})^2 = \mathbf{p} - 0.25\mathbf{p}^2$. Adding the probability that both neurons saturate towards 1, which is $(0.5\mathbf{p})^2 = 0.25\mathbf{p}^2$, the final probability of the neuron product saturation is $\mathbf{p} - 0.25\mathbf{p}^2 + 0.25\mathbf{p}^2 = \mathbf{p}$. Taking a product of sigmoid activated neurons therefore does not reduce the probability of neuron collapse.

Rectified Linear-Unit: In the case of a ReLU activation, the probability of a single neuron dying is taken as \mathbf{p} . As we look at the product of two neurons, the probability that one of the two neurons does not saturate is therefore $1 - \mathbf{p}$, and the probability that both neurons do not saturate is $(1 - \mathbf{p})^2$. The probability that at least one neuron saturates is thus equal to $1 - (1 - \mathbf{p})^2 = 2\mathbf{p} - \mathbf{p}^2$. As the ReLU saturation results in strict zeroes, this results in the product also being zero. Taking a product of ReLU activated neurons therefore increases the final neuron saturation probability from \mathbf{p} to $2\mathbf{p} - \mathbf{p}^2$. For an overview, we refer the reader to both Table 1 and the corresponding empirical evidence in Appendix C.3.

Table 1: Predicted dying neuron probabilities with and without a Hadamard representation.

Activation	Prob.	Prob. with HR	Δ
Tanh	\mathbf{p}	\mathbf{p}^2	$-(\mathbf{p} - \mathbf{p}^2)$
Sigmoid	\mathbf{p}	\mathbf{p}	0
ReLU	\mathbf{p}	$2\mathbf{p} - \mathbf{p}^2$	$+(\mathbf{p} - \mathbf{p}^2)$

5. Experiments

We analyze the effect of a Hadamard representation on a hidden layer’s fraction of dying neurons, its effective rank and the downstream performance. In the qualitative analysis, we evaluate DQN (Mnih et al., 2015) and PPO (Schulman et al., 2017) on 8 common, non-exploration driven Atari environments for 40M frames. Finally, a larger performance analysis is done using the recent Parallelized Q-Network

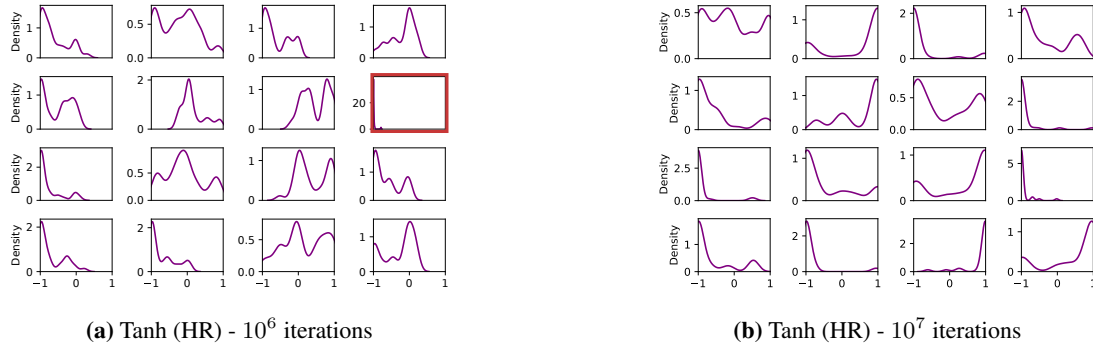


Figure 6: Kernel Density Estimations (KDE) over a subset of 16 neurons in the compressed representation z_t after training DQN in the Breakout environment using a Hadamard representation (HR) with hyperbolic tangents. The Hadamard representation tends to quickly utilize the full range of the hyperbolic tangent while also mitigating dying neurons.

(PQN) (Gallici et al., 2024) on 51 Atari environments for 40M frames.

Mitigating dying Hyperbolic Tangents

As defined in Eq. 1, the number of dead neurons is equal to the amount of neurons that display the same saturated output for any given observation s_t . Over 8 Atari environments, the average amount of dead neurons during training can be seen in Fig.7(a). For the ReLU activation, around 60% of the neurons in the representation z_t die during training, while for the sigmoid and hyperbolic tangent activation this number is around 40%. When using a hyperbolic tangent Hadamard representation, a reduction in dead neurons as compared to using a single hyperbolic tangent can be observed. We credit this to the inherent ability of a Hadamard product of hyperbolic tangents to minimize long-term activation saturation, as explained in Section 4. Quantitative results of dead neurons can be found in Table 2, which tends to confirm the predictions from Table 1. As compared to the Hadamard representation, layer normalization notably reduces dead hyperbolic tangents to an even lower value. Interestingly, the effects of layer normalization show that even if dead neurons are reduced more strongly, it does not always coincide with a higher effective rank (see Fig. 7(b)). On the other hand, the Hadamard representation does seem to have a positive effect on both metrics.

Table 2: Average dying neuron fractions in 8 Atari Games with and without a Hadamard representation (HR).

Activation	Without HR	With HR	Δ
Tanh	0.39	0.30	-23%
Sigmoid	0.44	0.45	+2%
ReLU	0.62	0.73	+18%

For more activation-specific dying neuron graphs, we refer

the reader to Appendix C.3.

Increasing Effective Rank

We additionally investigate the effective rank (Kumar et al., 2021) of the representation z_t during training, which can be seen in Fig. 7(b). As observed by Gulcehre et al. (2022), a representation activated by a hyperbolic tangent or a sigmoid, already has a relatively high effective rank compared to a representation activated by a ReLU. Furthermore, similar to the results in our supervised learning experiments (see Fig. 2), using a Hadamard representation with hyperbolic tangents significantly improves said effective rank, which is strongly correlated to a network’s ‘expressivity’. Alternatively, we found that employing a Hadamard representation with ReLU activations significantly decreased the effective rank of the representation, as was expected from earlier predictions in Table 1. More details on the ReLU Hadamard representation, dying neuron calculations and effective rank calculations can be found in Appendices C.4, B.1 and B.2, respectively.

Performance in Atari

The influence of a Hadamard representation on downstream performance is visualized in Fig. 7(c). Correlating with the reduction in dying neurons and an increase in effective rank, a significant improvement over the standard hyperbolic tangent baseline is obtained, as well as an improvement over the default ReLU baseline. Furthermore, a comparison is made with the novel Rational (Delfosse et al., 2024) activation function as the activation in the final hidden layer. Fig. 7(c) shows that, although the Rational activation seems to be a stable learnable activation, it remains comparable to the ReLU.

Examining further ablations in Fig. 8(a-b) shows that using another piece-wise linear function such as the SELU activation (Klambauer et al., 2017) or using an addition rather

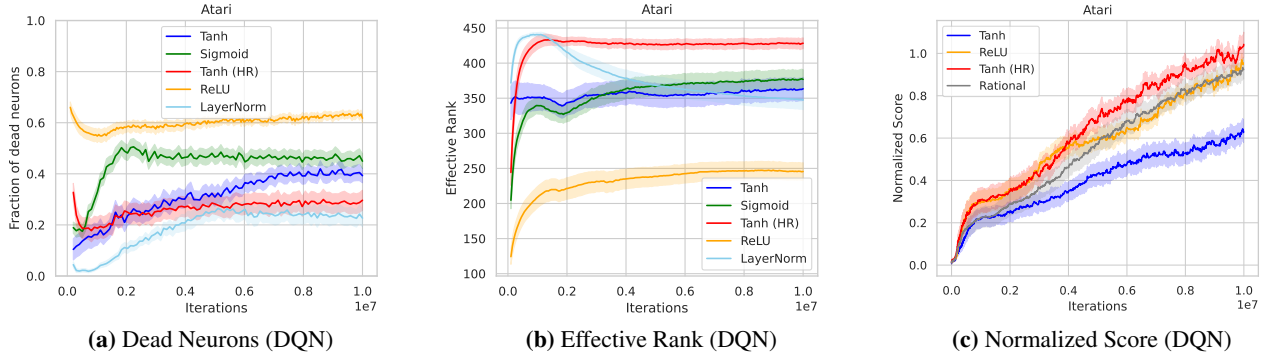


Figure 7: (a) The average fraction of dead neurons, (b) the average effective rank (Kumar et al., 2021), and (c) the baseline-normalized score when training DQN in the Atari domain for 10M iterations (40M frames). Similar to the well-known dying ReLU problem, hyperbolic tangent and sigmoid activations also exhibit strong dying neuron behavior. A Hadamard product of hyperbolic tangents reduces dead neurons in z_t and subsequently increases the effective rank of the representation.

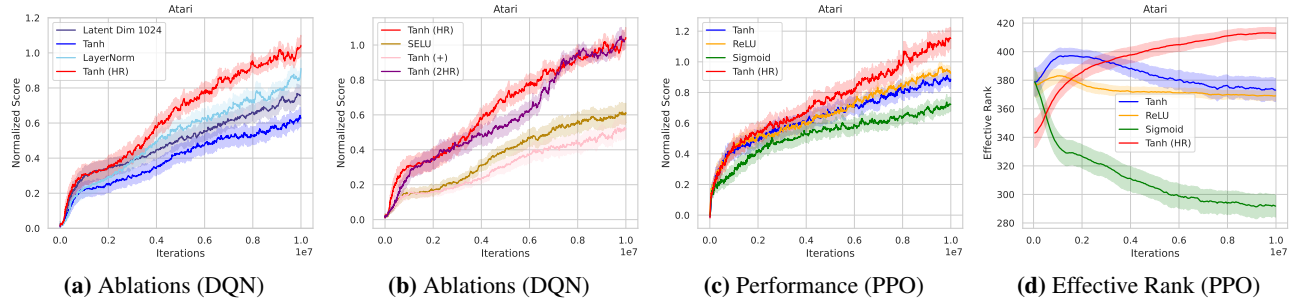


Figure 8: Baseline-normalized performance with the standard deviation over the means in the Atari domain, after training DQN for 10M iterations (40M Frames). In (a), Tanh (HR) significantly outperforms Tanh. The Rational Activation (Delfosse et al., 2024) is comparable to ReLU within 40M frames. In (b), several ablations including layer normalization (Ba et al., 2016) and an increased dimension of $z_t \in \mathbb{R}^{1024}$ with a reduced learning rate $\alpha = 5e-5$ are shown. In b), Tanh (+) represents an addition rather than a Hadamard product, and Tanh (2HR) uses a triple Hadamard product. Normalized performance (c) and effective rank (d) when training the PPO algorithm (Schulman et al., 2017). Note that no hyperparameter changes are done for the Hadamard representation.

than a product of hyperbolic tangents seems detrimental to performance. Furthermore, taking a product of 3 hyperbolic tangents (2HR) also appears to enhance performance, though there seems to be a negative effect in the early stages of training as compared to using a single Hadamard product. We hypothesize that this is the result of increased contracting behavior in the early stage of training due to increasing multiplication of hyperbolic tangent activations whose absolute values are < 1 . Additional experiments combining the ReLU activation with a Hadamard representation can be found in Appendix C.4.

The Immunity of the ReLU

Interestingly, it seems that the ReLU activation’s performance is much less correlated to its low effective rank and high amount of dying neurons than the continuously differentiable activations. As also indicated by Teney et al.

(2024), the exact reasons for the broad success of the ReLU activations are not yet fully understood. However, we have offered a partial explanation for this resilience of the ReLU in Section 4: ReLU saturation represents network pruning while hyperbolic tangent saturation leads to biases in subsequent layers.

Evaluating Hadamard representations on PPO

To evaluate results on a policy-based algorithm, additional experiments are run using the PPO algorithm (Schulman et al., 2017). For PPO, the internal architectural difference with DQN and PQN is that the final hidden layer z_t precedes both a critic and an actor network, and thus receives policy and value gradients. After training for 40M frames, the performance and effective rank over time can be found in Fig. 8(c-d). Similarly to the results on DQN, the Tanh (HR) exhibits the highest effective rank and good performance.

The Tanh (HR) and the ReLU seem to have consistent strong performance, whereas the pure hyperbolic tangent and sigmoid activations can be unreliable across algorithms. This is coherent with the fact that continuously differentiable activations are generally not favored over the ReLU (Teney et al., 2024).

Evaluating Hadamard representations on PQN

To test the performance of the Hadamard representation over a broader selection of environments, we evaluate the recent Parallelized Q-Network (PQN) algorithm in the nearly full Atari suite without hard-exploration environments, for a total of 51 games with 5 seeds per game.

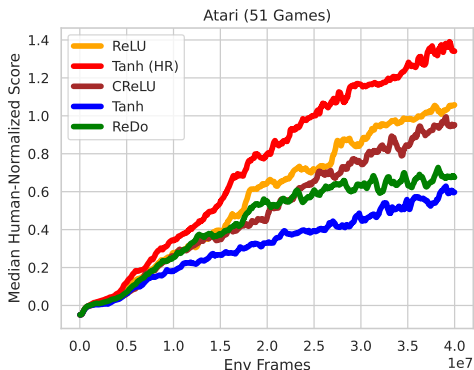


Figure 9: Median Human-Normalized scores on PQN in 51 Atari games for 5 seeds over 40M frames. Labels represent encoder activations. Employing a Hadamard representation provides a significant performance improvement over the recent PQN baseline (displayed as ReLU), the CReLU (Abbas et al., 2023) and ReDo ($\tau = 0.025$) (Sokar et al., 2023). Notably, the improvement over a conventionally parameterized hyperbolic tangent activation is more than 100%.

PQN is a vectorized-friendly version of DQN, reporting both a speed up from DQN as well as better convergence (Gallici et al., 2024). We run tests implementing the Hadamard representation in all hidden layers. The median human-normalized scores after training for 40M frames are shown in Fig. 9. We can clearly see a similar trend for the 51-game Atari suite. Using a Hadamard representation significantly increases the median performance as compared to the baseline PQN, the CReLU activation (Abbas et al., 2023), and the ReDo + ReLU algorithm (Sokar et al., 2023). Additionally, preliminary modified applications of ReDo to Tanh did not prove to be effective in PQN. However, we believe that future work in this direction would be worth pursuing.

6. Limitations

Using a Hadamard representation increases neural network parameters as it doubles the incoming weights connected

to a hidden layer. However, in Fig. 9, a comparison against the CReLU is shown, which also nearly doubles the network’s parameters. Furthermore, recent work shows that simply scaling baselines in Atari often leads to reduced performance (Obando-Ceron et al., 2024; Obando Ceron et al., 2024). Another limitation is that, due to the vast amount of activation functions and the theoretical sound candidacy of the hyperbolic tangent, our research focused on the combination of hyperbolic tangents. Further research into Hadamard representations could find more novel activation combinations. A hyperparameter search will also give more insights into the strengths of the HR, as all baselines are specifically tuned for the ReLU. Finally, integration of a HR into more complex algorithms and architectures such as Rainbow (Hessel et al., 2018), Impala (Espeholt et al., 2018) or SPR Schwarzer et al. (2021) would be interesting.

Table 3: Parameter count across different activations

Activation	Total Parameters
Tanh (Width:2)	6,717,376
Tanh (HR)	3,373,382
CReLU	3,292,838

7. Conclusions and Discussion

This paper analyzed issues with continuously differentiable activations in RL and demonstrated that these activation functions also suffer from the dying neuron problem, but with more acute downstream effects. To alleviate this problem and make better use of these functions’ properties, a novel representation architecture called the Hadamard representation (HR) is proposed. The HR augments the hidden layers in a network by taking the Hadamard product with parallel, independently parameterized activation layers. We further analyzed and empirically showed that applying a Hadamard representation to hyperbolic tangents reduces the occurrence of dead neurons in the representation and increases layer expressiveness. In DQN, PQN and PPO, this approach significantly improved performance in Atari games compared to both standard representation parameterization and merely increasing the representation dimension. Future work could focus on further identifying the intricacies of the effects that different activation functions have on the resulting representation, in an attempt to push the potential of non piece-wise linear activations in reinforcement learning or even in a supervised learning setting (see Fig. 2). Also, we believe that an implementation of Hadamard-style architectures in a continual learning setting as in Abbas et al. (2023) or in Delfosse et al. (2024) could be promising.

References

- Abbas, Z., Zhao, R., Modayil, J., White, A., and Machado, M. C. Loss of plasticity in continual deep reinforcement learning. In Chandar, S., Pascanu, R., Sedghi, H., and Precup, D. (eds.), *Proceedings of The 2nd Conference on Lifelong Learning Agents*, volume 232 of *Proceedings of Machine Learning Research*, pp. 620–636. PMLR, 22–25 Aug 2023. URL <https://proceedings.mlr.press/v232/abbas23a.html>.
- Arnob, S. Y., Ohib, R., Plis, S. M., and Precup, D. Single-shot pruning for offline reinforcement learning. *CoRR*, abs/2112.15579, 2021. URL <https://arxiv.org/abs/2112.15579>.
- Ba, J. L., Kiros, J. R., and Hinton, G. E. Layer normalization, 2016. URL <http://arxiv.org/abs/1607.06450>. cite arxiv:1607.06450.
- Bjorck, J., Gomes, C. P., and Weinberger, K. Q. Is high variance unavoidable in RL? a case study in continuous control. In *International Conference on Learning Representations*, 2022. URL <https://openreview.net/forum?id=9xhgmsNVHu>.
- Dauphin, Y. N., Fan, A., Auli, M., and Grangier, D. Language modeling with gated convolutional networks. In Precup, D. and Teh, Y. W. (eds.), *Proceedings of the 34th International Conference on Machine Learning*, volume 70 of *Proceedings of Machine Learning Research*, pp. 933–941. PMLR, 06–11 Aug 2017. URL <https://proceedings.mlr.press/v70/dauphin17a.html>.
- Delfosse, Q., Schramowski, P., Mundt, M., Molina, A., and Kersting, K. Adaptive rational activations to boost deep reinforcement learning. In *The Twelfth International Conference on Learning Representations*, 2024. URL <https://openreview.net/forum?id=g90ysX1sVs>.
- Dohare, S., Hernandez-Garcia, J. F., Lan, Q., Rahman, P., Mahmood, A. R., and Sutton, R. S. Loss of plasticity in deep continual learning. *Nature*, 632(8026): 768–774, 2024. ISSN 1476-4687. doi: 10.1038/s41586-024-07711-7. URL <https://doi.org/10.1038/s41586-024-07711-7>.
- Dubey, S. R., Singh, S. K., and Chaudhuri, B. B. Activation functions in deep learning: A comprehensive survey and benchmark. *Neurocomputing*, 503:92–108, 2022. ISSN 0925-2312. doi: <https://doi.org/10.1016/j.neucom.2022.06.111>. URL <https://www.sciencedirect.com/science/article/pii/S0925231222008426>.
- Espeholt, L., Soyer, H., Munos, R., Simonyan, K., Mnih, V., Ward, T., Doron, Y., Firoiu, V., Harley, T., Dunning, I., Legg, S., and Kavukcuoglu, K. IMPALA: Scalable distributed deep-RL with importance weighted actor-learner architectures. In Dy, J. and Krause, A. (eds.), *Proceedings of the 35th International Conference on Machine Learning*, volume 80 of *Proceedings of Machine Learning Research*, pp. 1407–1416. PMLR, 10–15 Jul 2018. URL <https://proceedings.mlr.press/v80/espeholt18a.html>.
- Fukushima, K. Visual feature extraction by a multilayered network of analog threshold elements. *IEEE Transactions on Systems Science and Cybernetics*, 5(4):322–333, 1969. doi: 10.1109/TSSC.1969.300225.
- Gallici, M., Fellows, M., Ellis, B., Pou, B., Masmitja, I., Foerster, J. N., and Martin, M. Simplifying deep temporal difference learning, 2024. URL <https://arxiv.org/abs/2407.04811>.
- Glorot, X. and Bengio, Y. Understanding the difficulty of training deep feedforward neural networks. In Teh, Y. W. and Titterton, M. (eds.), *Proceedings of the Thirteenth International Conference on Artificial Intelligence and Statistics*, volume 9 of *Proceedings of Machine Learning Research*, pp. 249–256, Chia Laguna Resort, Sardinia, Italy, 13–15 May 2010. PMLR. URL <https://proceedings.mlr.press/v9/glorot10a.html>.
- Goodfellow, I., Bengio, Y., and Courville, A. *Deep Learning*. Adaptive computation and machine learning. MIT Press, 2016. ISBN 9780262035613. URL <https://books.google.co.in/books?id=Np9SDQAAQBAJ>.
- Graesser, L., Evci, U., Elsen, E., and Castro, P. S. The state of sparse training in deep reinforcement learning. In Chaudhuri, K., Jegelka, S., Song, L., Szepesvari, C., Niu, G., and Sabato, S. (eds.), *Proceedings of the 39th International Conference on Machine Learning*, volume 162 of *Proceedings of Machine Learning Research*, pp. 7766–7792. PMLR, 17–23 Jul 2022. URL <https://proceedings.mlr.press/v162/graesser22a.html>.
- Grooten, B., Tomilin, T., Vasan, G., Taylor, M. E., Mahmood, A. R., Fang, M., Pechenizkiy, M., and Mocanu, D. C. Madi: Learning to mask distractions for generalization in visual deep reinforcement learning. In *International Conference on Autonomous Agents and Multiagent Systems*, AAMAS, 2024.
- Gulcehre, C., Srinivasan, S., Sygnowski, J., Ostrovski, G., Farajtabar, M., Hoffman, M., Pascanu, R., and

- Doucet, A. An empirical study of implicit regularization in deep offline RL. *Transactions on Machine Learning Research*, 2022. ISSN 2835-8856. URL <https://openreview.net/forum?id=HFfJWx60IT>.
- He, K., Zhang, X., Ren, S., and Sun, J. Delving deep into rectifiers: Surpassing human-level performance on imagenet classification. In *Proceedings of the IEEE international conference on computer vision*, pp. 1026–1034, 2015.
- He, K., Zhang, X., Ren, S., and Sun, J. Deep Residual Learning for Image Recognition. In *Proceedings of 2016 IEEE Conference on Computer Vision and Pattern Recognition*, CVPR '16, pp. 770–778. IEEE, June 2016. doi: 10.1109/CVPR.2016.90. URL <http://ieeexplore.ieee.org/document/7780459>.
- Henderson, P., Islam, R., Bachman, P., Pineau, J., Precup, D., and Meger, D. Deep reinforcement learning that matters. In *Proceedings of the Thirty-Second AAAI Conference on Artificial Intelligence and Thirtieth Innovative Applications of Artificial Intelligence Conference and Eighth AAAI Symposium on Educational Advances in Artificial Intelligence*, AAAI'18/IAAI'18/EAAI'18. AAAI Press, 2018. ISBN 978-1-57735-800-8.
- Hessel, M., Modayil, J., van Hasselt, H., Schaul, T., Ostrovski, G., Dabney, W., Horgan, D., Piot, B., Azar, M. G., and Silver, D. Rainbow: Combining improvements in deep reinforcement learning. In McIlraith, S. A. and Weinberger, K. Q. (eds.), *AAAI*, pp. 3215–3222. AAAI Press, 2018. URL <http://dblp.uni-trier.de/db/conf/aaai/aaai2018.html#HesselMHsODHPAS18>.
- Hochreiter, S. and Schmidhuber, J. Long short-term memory. *Neural Computation*, 9(8):1735–1780, 1997. doi: 10.1162/neco.1997.9.8.1735.
- Huang, S., Dossa, R. F. J., Ye, C., Braga, J., Chakraborty, D., Mehta, K., and Araújo, J. G. Cleanrl: High-quality single-file implementations of deep reinforcement learning algorithms. *Journal of Machine Learning Research*, 23(274): 1–18, 2022. URL <http://jmlr.org/papers/v23/21-1342.html>.
- Jarrett, K., Kavukcuoglu, K., Ranzato, M., and LeCun, Y. What is the best multi-stage architecture for object recognition? In *2009 IEEE 12th International Conference on Computer Vision*, pp. 2146–2153, 2009. doi: 10.1109/ICCV.2009.5459469.
- Klambauer, G., Unterthiner, T., Mayr, A., and Hochreiter, S. Self-normalizing neural networks. In *Advances in Neural Information Processing Systems 30: Annual Conference on Neural Information Processing Systems 2017*, December 4-9, 2017, Long Beach, CA, USA, pp. 971–980, 2017.
- Kumar, A., Agarwal, R., Ghosh, D., and Levine, S. Implicit under-parameterization inhibits data-efficient deep reinforcement learning. In *International Conference on Learning Representations*, 2021.
- Liu, V., Kumaraswamy, R., Le, L., and White, M. The utility of sparse representations for control in reinforcement learning. In *Proceedings of the Thirty-Third AAAI Conference on Artificial Intelligence and Thirty-First Innovative Applications of Artificial Intelligence Conference and Ninth AAAI Symposium on Educational Advances in Artificial Intelligence*, AAAI'19/IAAI'19/EAAI'19. AAAI Press, 2019. ISBN 978-1-57735-809-1. doi: 10.1609/aaai.v33i01.33014384. URL <https://doi.org/10.1609/aaai.v33i01.33014384>.
- Lu, L., Shin, Y., Su, Y., and Karniadakis, G. E. Dying relu and initialization: Theory and numerical examples. *CoRR*, abs/1903.06733, 2019. URL <http://dblp.uni-trier.de/db/journals/corr/corr1903.html#abs-1903-06733>.
- Lyle, C., Rowland, M., and Dabney, W. Understanding and preventing capacity loss in reinforcement learning. In *International Conference on Learning Representations*, 2022. URL <https://openreview.net/forum?id=ZkC8wKoLbQ7>.
- Mnih, V., Kavukcuoglu, K., Silver, D., et al. Human-level control through deep reinforcement learning. *Nature*, 518 (7540):529–533, 2 2015. doi: 10.1038/nature14236.
- Molina, A., Schramowski, P., and Kersting, K. Padé activation units: End-to-end learning of flexible activation functions in deep networks. In *International Conference on Learning Representations*, 2019.
- Nair, V. and Hinton, G. E. Rectified linear units improve restricted boltzmann machines. In *ICML 2010*, pp. 807–814, 2010.
- Nikishin, E., Schwarzer, M., D’Oro, P., Bacon, P.-L., and Courville, A. The primacy bias in deep reinforcement learning. In Chaudhuri, K., Jegelka, S., Song, L., Szepesvari, C., Niu, G., and Sabato, S. (eds.), *Proceedings of the 39th International Conference on Machine Learning*, volume 162 of *Proceedings of Machine Learning Research*, pp. 16828–16847. PMLR, 17–23 Jul 2022.
- Nikishin, E., Oh, J., Ostrovski, G., Lyle, C., Pascanu, R., Dabney, W., and Barreto, A. Deep reinforcement learning with plasticity injection. In Oh, A., Naumann, T., Globerson, A., Saenko, K., Hardt, M., and Levine, S.

- (eds.), *Advances in Neural Information Processing Systems*, volume 36, pp. 37142–37159. Curran Associates, Inc., 2023.
- Obando-Ceron, J., Courville, A., and Castro, P. S. In deep reinforcement learning, a pruned network is a good network. *arXiv preprint arXiv:2402.12479*, 2024.
- Obando Ceron, J. S., Sokar, G., Willi, T., Lyle, C., Farebrother, J., Foerster, J. N., Dziugaite, G. K., Precup, D., and Castro, P. S. Mixtures of experts unlock parameter scaling for deep RL. In Salakhutdinov, R., Kolter, Z., Heller, K., Weller, A., Oliver, N., Scarlett, J., and Berkenkamp, F. (eds.), *Proceedings of the 41st International Conference on Machine Learning*, volume 235 of *Proceedings of Machine Learning Research*, pp. 38520–38540. PMLR, 21–27 Jul 2024. URL <https://proceedings.mlr.press/v235/obando-ceron24b.html>.
- Schulman, J., Wolski, F., Dhariwal, P., Radford, A., and Klimov, O. Proximal policy optimization algorithms. *ArXiv*, abs/1707.06347, 2017. URL <https://api.semanticscholar.org/CorpusID:28695052>.
- Schwarzer, M., Anand, A., Goel, R., Hjelm, R. D., Courville, A., and Bachman, P. Data-Efficient Reinforcement Learning with Self-Predictive Representations. In *International Conference on Learning Representations, ICLR*, 2021.
- Shang, W., Sohn, K., Almeida, D., and Lee, H. Understanding and improving convolutional neural networks via concatenated rectified linear units. In Balcan, M. F. and Weinberger, K. Q. (eds.), *Proceedings of The 33rd International Conference on Machine Learning*, volume 48 of *Proceedings of Machine Learning Research*, pp. 2217–2225, New York, New York, USA, 20–22 Jun 2016. PMLR. URL <https://proceedings.mlr.press/v48/shang16.html>.
- Silverman, B. W. *Density Estimation for Statistics and Data Analysis*. Chapman and Hall, 1986.
- Sokar, G., Mocanu, E., Mocanu, D. C., Pechenizkiy, M., and Stone, P. Dynamic sparse training for deep reinforcement learning. In Raedt, L. D. (ed.), *Proceedings of the Thirty-First International Joint Conference on Artificial Intelligence, IJCAI-22*, pp. 3437–3443. International Joint Conferences on Artificial Intelligence Organization, 7 2022. doi: 10.24963/ijcai.2022/477. URL <https://doi.org/10.24963/ijcai.2022/477>. Main Track.
- Sokar, G., Agarwal, R., Castro, P. S., and Evci, U. The dormant neuron phenomenon in deep reinforcement learning. In *Proceedings of the 40th International Conference on Machine Learning, ICML’23*. JMLR.org, 2023.
- Srivastava, R. K., Greff, K., and Schmidhuber, J. Training very deep networks. In Cortes, C., Lawrence, N., Lee, D., Sugiyama, M., and Garnett, R. (eds.), *Advances in Neural Information Processing Systems*, volume 28. Curran Associates, Inc., 2015. URL https://proceedings.neurips.cc/paper_files/paper/2015/file/215a71a12769b056c3c32e7299f1c5ed-Paper.pdf.
- Sutton, R. S. and Barto, A. G. *Reinforcement Learning: An Introduction*. The MIT Press, second edition, 2018. URL <http://incompleteideas.net/book/the-book-2nd.html>.
- Tan, Y., Hu, P., Pan, L., Huang, J., and Huang, L. RLx2: Training a sparse deep reinforcement learning model from scratch. *CoRR*, abs/2205.15043, 2023. URL <https://arxiv.org/abs/2205.15043>.
- Teney, D., Nicolicioiu, A. M., Hartmann, V., and Abbasnejad, E. Neural redshift: Random networks are not random functions. In *Proceedings of the IEEE/CVF Conference on Computer Vision and Pattern Recognition (CVPR)*, pp. 4786–4796, June 2024.
- Xu, B., Wang, N., Chen, T., and Li, M. Empirical evaluation of rectified activations in convolutional network. *CoRR*, abs/1505.00853, 2015. URL <http://arxiv.org/abs/1505.00853>.

A. Implementation Details

A.1. Hyperparameters

To evaluate, 8 different Atari environments are tested, using 5 different random seeds. For the mean scores, we take the mean over the eight environments. Our normalized score is calculated according to our baseline, the original implementation using a ReLU activation.

All the hyperparameters used in our experiments for DQN and PPO, respectively, are as reported in `cleanrl` (Huang et al., 2022). The hyperparameters can be found in Table 1 and Table 2.

Table 4: DQN Hyperparameters

Hyperparameter	Value	Description
Learning Rate	1×10^{-4}	Learning rate for the optimizer
Discount Factor (γ)	0.99	Discount for future rewards
Replay Memory Size	1,000,000	Size of the experience replay buffer
Mini-batch Size	32	Number of samples per batch update
Target Network Update Frequency	1000	Update frequency for the target network
Initial Exploration	1.0	Initial exploration rate in ϵ -greedy
Final Exploration	0.1	Final exploration rate in ϵ -greedy
Final Exploration Frame	1,000,000	Frame number to reach final exploration
Exploration Decay Frame	1,000,000	Frames over which exploration rate decays
Action Repeat (Frame Skip)	4	Number of frames skipped per action
Reward Clipping	[-1, 1]	Range to which rewards are clipped
Input Dimension	84 x 84	Dimensions of the input image
Latent Dimension	512	Dimension of the latent representation
Input Frames	4	Number of frames used as input
Training Start Frame	80,000	Frame number to start training
Loss Function	Mean Squared Error	Loss function used for updates
Optimizer	Adam	Optimization algorithm used
Optimizer ϵ	10^{-5}	Adam Epsilon

Table 5: PPO Hyperparameters

Hyperparameter	Value	Description
Learning Rate	2.5×10^{-4}	Learning rate for the optimizer
Discount Factor (γ)	0.99	Discount factor for future rewards
Number of Steps	128	Number of steps per environment before update
Anneal LR	True	Whether to anneal the learning rate
GAE Lambda	0.95	Lambda parameter for GAE
Number of Minibatches	4	Number of minibatches to split the data
Update Epochs	4	Number of epochs per update
Normalize Advantage	True	Whether to normalize advantage estimates
Clipping Coefficient	0.1	Clipping parameter for PPO
Clip Value Loss	True	Whether to clip value loss
Entropy Coefficient	0.01	Coefficient for entropy bonus
Value Function Coefficient	0.5	Coefficient for value function loss
Maximum Gradient Norm	0.5	Maximum norm for gradient clipping
Target KL	None	Target KL divergence between updates
Latent Dimension	512	Dimension of the latent representation
Optimizer	Adam	Optimization algorithm used
Optimizer ϵ	10^{-5}	Adam Epsilon

Table 6: PQN Hyperparameters (Gallici et al., 2024)

Hyperparameter	Value	Description
Total Timesteps	10,000,000	Total timesteps for training
Timesteps for Decay	10,000,000	Timesteps for decay functions (epsilon and lr)
Number of Environments	128	Number of parallel environments
Steps per Environment	32	Steps per environment in each update
Number of Epochs	2	Number of epochs per update
Number of Minibatches	32	Number of minibatches per epoch
Starting Epsilon	1.0	Starting epsilon for exploration
Final Epsilon	0.001	Final epsilon for exploration
Epsilon Decay Ratio	0.1	Decay ratio for epsilon
Epsilon for Test Policy	0.0	Epsilon for greedy test policy
Learning Rate	0.00025	Learning rate
Learning Rate Linear Decay	True	Use linear decay for learning rate
Max Gradient Norm	10.0	Max gradient norm for clipping
Discount Factor (γ)	0.99	Discount factor for reward
Lambda (λ)	0.65	Lambda for generalized advantage estimation
Episodic Life	True	Terminate episode when life is lost
Reward Clipping	True	Clip rewards to range [-1, 1]
Frame Skip	4	Number of frames to skip
Max No-Ops on Reset	30	Max number of no-ops on reset
Test During Training	True	Run evaluation during training
Number of Test Envs	8	Number of environments used for testing

A.2. Hadamard Implementation

Constructing a Hadamard representation is a straightforward process that only requires additional, parallel incoming weights. Starting from a hidden layer, the Pytorch pseudocode is defined as follows:

```
# hidden = previous hidden layer
linear1 = nn.Linear(input_dim, output_dim)
linear2 = nn.Linear(input_dim, output_dim)
representation1 = nn.Tanh(linear1(hidden))
representation2 = nn.Tanh(linear2(hidden))
hadamard_representation = representation1 * representation2
```

A.3. Reinforcement Learning

In DQN, the action a_t is chosen following an ϵ -greedy policy. With probability ϵ , a random action is selected, and with $(1 - \epsilon)$, the action maximizing the Q-value is chosen. The target Y_t is defined as:

$$Y_t = r_t + \gamma Q'(z_{t+1}, \underset{a \in \mathcal{A}}{\operatorname{argmax}} Q(z_{t+1}, a)), \quad (5)$$

where $Q'(z, a)$ denotes the target Q-network, an auxiliary network that stabilizes the learning by providing a stable target for $Q(z, a)$. The parameters of Q' are updated less frequently to enhance learning stability. The loss function for training the network is:

$$\mathcal{L}_Q = |Y_t - Q(z_t, a)|^2. \quad (6)$$

Proximal Policy Optimization (PPO) operates on a different principle, utilizing policy gradient methods for policy improvement. PPO seeks to update the policy by maximizing an objective function while preventing large deviations from the previous policy through a clipping mechanism in the objective's estimator. The clipped policy gradient loss L^{CLIP} is defined as:

$$L^{CLIP}(\theta) = \mathbb{E} \left[\min(r_t(\theta)\hat{A}_t, \operatorname{clip}(r_t(\theta), 1 - \epsilon, 1 + \epsilon)\hat{A}_t) \right], \quad (7)$$

where $r_t(\theta)$ represents the ratio of the probabilities under the new policy versus the old policy, and \hat{A}_t is the advantage estimate at timestep t . This clipped surrogate objective ensures gradual and stable policy updates.

B. Kernel Density Estimations

As discussed in Section 4, we hypothesize that the differences between a hyperbolic tangent with and without an HR are due to the increased ability of the product of hyperbolic tangents being able to negate dying neurons. We further see this phenomenon when plotting a random selection of neurons from both the mask and the base representation in Fig. 10(a).

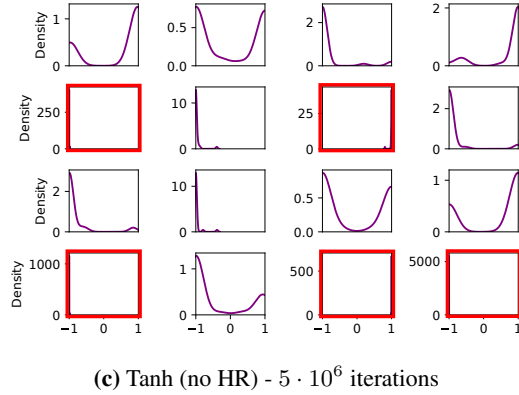
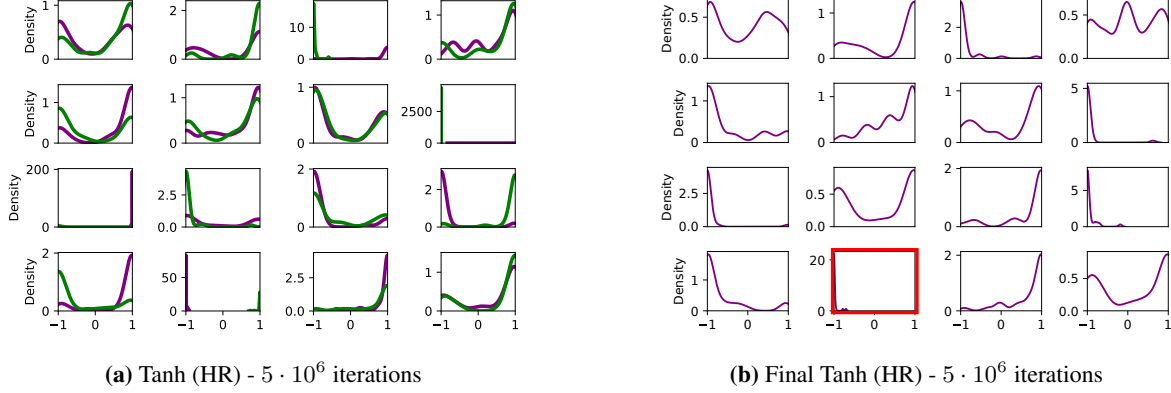


Figure 10: Kernel Density Estimations (KDE) over a subset of 16 neurons in the representations z_t^{enc} and z_t^* in (a), the resulting Hadamard product z_t in (b) and the representation z_t when training without an HR (c). These representations are obtained after training DQN in the 'Breakout' environment. Red outlines represent dead (collapsed) neurons. In (a), a closer look at neurons 3, 8 and 9 shows that when one of the representations saturates, the other is able to compensate, leading to a non-dead neuron in their product z_t in (b).

B.1. KDE calculation

Firstly, to stabilize the KDE computation and avoid singularity issues, a small noise ϵ , following a normal distribution, is added to each neuron's activations:

$$\alpha'_i = \alpha_i + \epsilon, \quad \epsilon \sim \mathcal{N}(0, \sigma^2)$$

where $\sigma^2 = 1 \times 10^{-5}$. The bandwidth for KDE, crucial for the accuracy of the density estimate, is calculated using Scott's rule, adjusted by the standard deviation of the jittered activations:

$$bw = n^{-\frac{1}{5}} \cdot \text{std}(\alpha'_i)$$

where n is the number of samples in α_i . The density of activations is then estimated using a Gaussian kernel:

$$f(x) = \frac{1}{n \cdot bw} \sum_{j=1}^n K\left(\frac{x - \alpha'_{ij}}{bw}\right)$$

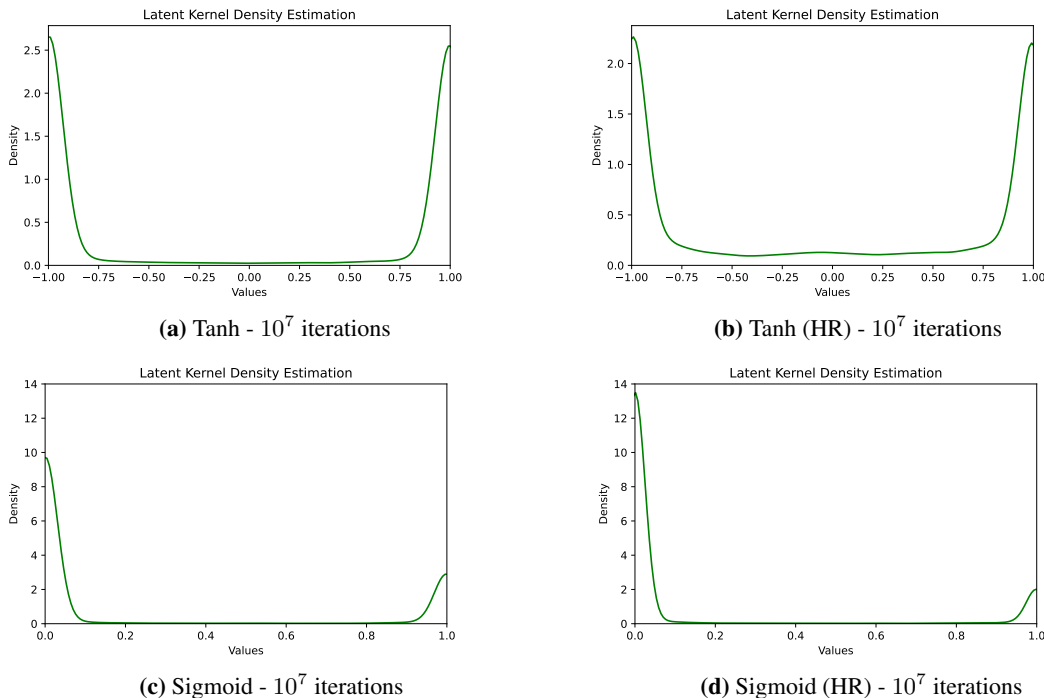


Figure 11: Kernel Density Estimations of the final representation z_t after training DQN for 10^7 iterations in the Breakout environment. A hyperbolic tangent Hadamard representation allows the representation to avoid strong saturation, keeping sufficient kernel density in the central sections of the hyperbolic tangent. As a sigmoid can saturate into zero, using a Hadamard representation remains less effective for preventing saturation, as any zero will lead to a Hadamard product of zero.

Here, K denotes the Gaussian kernel function. In order to finally determine if a neuron is dead, the maximum value of the estimated density function $f(x)$ is compared against a predefined threshold:

$$\max(f(x)) \geq \omega$$

where ω represents the predetermined threshold. In practice, after analyzing the individual neuron KDE’s, using an ω of 20 provides a strong approximation of actual dead neurons.

B.2. Effective Rank calculation

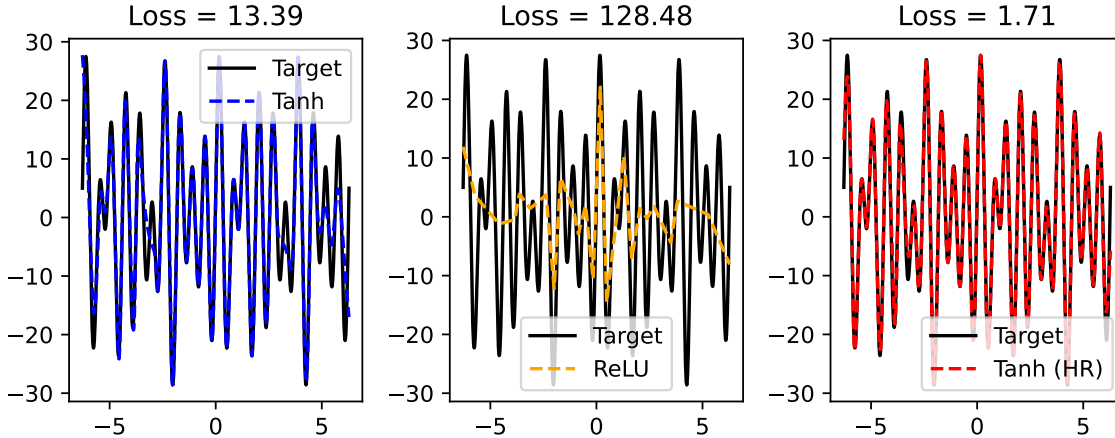
In line with Kumar et al. (2021), the effective rank of a feature matrix for a threshold δ ($\delta = 0.01$), denoted as $srank_\delta(\Phi)$, is given by $srank_\delta(\Phi) = \min \left\{ k : \frac{\sum_{i=1}^k \sigma_i(\Phi)}{\sum_{i=1}^d \sigma_i(\Phi)} \geq 1 - \delta \right\}$, where $\{\sigma_i(\Phi)\}$ are the singular values of Φ in decreasing order, i.e., $\sigma_1 \geq \dots \geq \sigma_d \geq 0$. Intuitively, the effective rank of a feature matrix represents the number of “effective” unique components that form the basis for linearly approximating the resulting Q-values. The calculation in Python is done as follows:

```
def compute_rank_from_features(feature_matrix, rank_delta=0.01):
    sing_values = np.linalg.svd(feature_matrix, compute_uv=False)
    cumsum = np.cumsum(sing_values)
    nuclear_norm = np.sum(sing_values)
    approximate_rank_threshold = 1.0 - rank_delta
    threshold_crossed = (cumsum >= approximate_rank_threshold * nuclear_norm)
    effective_rank = sing_values.shape[0] - np.sum(threshold_crossed) + 1
    return effective_rank
```

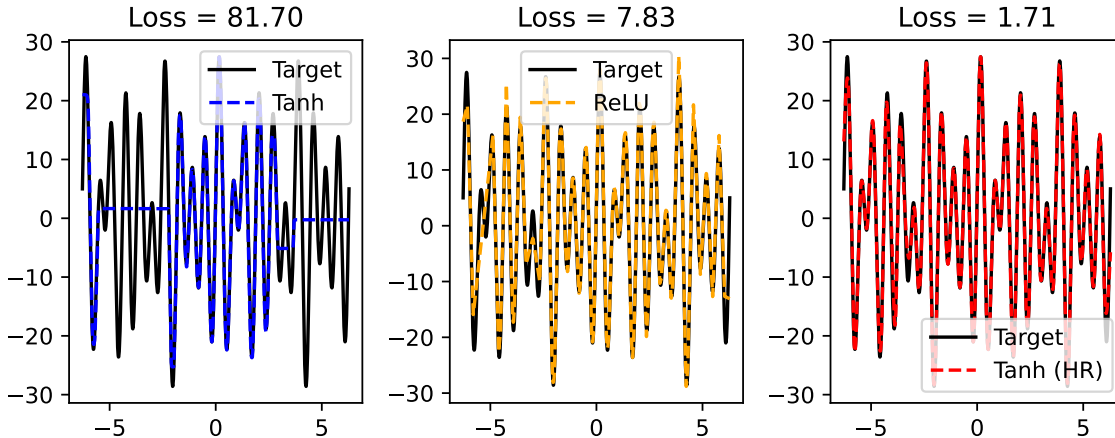
C. Additional Experiments

C.1. Shallow and Deep Function Approximation

To further showcase the effect of activations on complex function approximation, we compare the single hidden layer Tanh (HR) network from Fig. 2 with a deep ReLU and Tanh network containing three hidden layers each. The comparison with shallow networks can be found in Fig. 12(a) and a comparison with deep networks can be found in Fig. 12(b).



(a) Comparison of shallow networks for a nonlinear regression task. The Tanh and ReLU networks have a single hidden layer of 200 neurons, while the Tanh (HR) has a single hidden layer of 100 neurons but two preceding linear layers. The Tanh and ReLU networks have 601 parameters, while the Tanh (HR) network has 501 parameters. As found by Gulcehre et al. (2022), a shallow network activated by ReLU has a lower effective rank and consequently reduced network expressivity as compared to a Tanh activated network. Using a Hadamard representation, we achieve better function approximation while using less parameters.



(b) Comparison of two deep networks and one shallow network for the same nonlinear regression task. The Tanh and ReLU networks have 3 hidden layers of 200 neurons each, while the Tanh (HR) network remains shallow. In line with common observations in deep learning, the ReLU activation thrives in deeper networks, in contrast to the Tanh activation. Interestingly, the shallow Tanh (HR) network still achieves better function approximation with only 0.6% of the deeper networks' parameters (81001 vs 501). No hyperparameter tuning or architecture search has been applied. Additional tests using deep Tanh (HR) networks gave similar function approximation as compared to the shallow Tanh (HR) network.

C.2. Increasing Representation Parameters

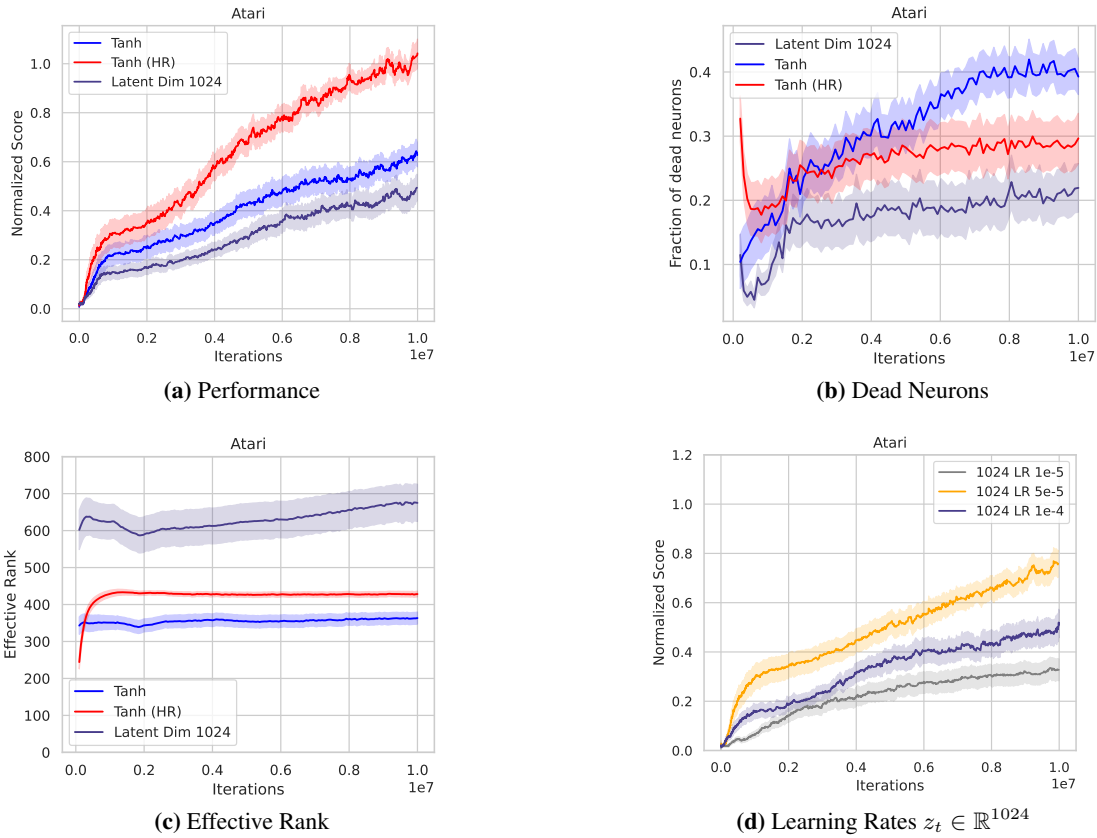


Figure 13: Comparison of a normal hyperbolic tangent (Tanh), a hyperbolic tangent with a higher representation dimension $z_t \in \mathbb{R}^{512 \rightarrow 1024}$ and a Hadamard representation using hyperbolic tangents. Comparisons are done on performance (a), the fraction of dead neurons (b), the effective rank of the representation z_t (c) and learning rates of the higher-dimensional latent. Naturally, increasing the representation dimension z_t increases the effective rank of the representation, but using a larger representation dimension is not always preferable as it often requires different hyperparameters, and can lead to reduced performance (Obando-Ceron et al., 2024; Obando Ceron et al., 2024). In (d), an ablation of learning rates shows that using a larger layer can sometimes prefer lower learning rates. However, it also shows that the improvement due to the Hadamard representation is likely not correlated with the parameter increase, as the Hadamard representation still significantly outperforms any of the 1024-dimensional latent state learning rate ablations.

C.3. Validating dying neuron probability derivations

As discussed in Section 4, the effect of using a Hadamard representation strongly depends on the activation function. These derivations are empirically validated by the results in Fig. 14. In practice, since a neural network prefers symmetry, a sigmoid saturates slightly faster to 0 than to 1. This could explain the very slight increase in dead neurons when using an HR with activations. Note that, since we use neuron independence assumptions in our theoretically calculated dying neuron probabilities, the empirical results differ in magnitude from the theoretical predictions.

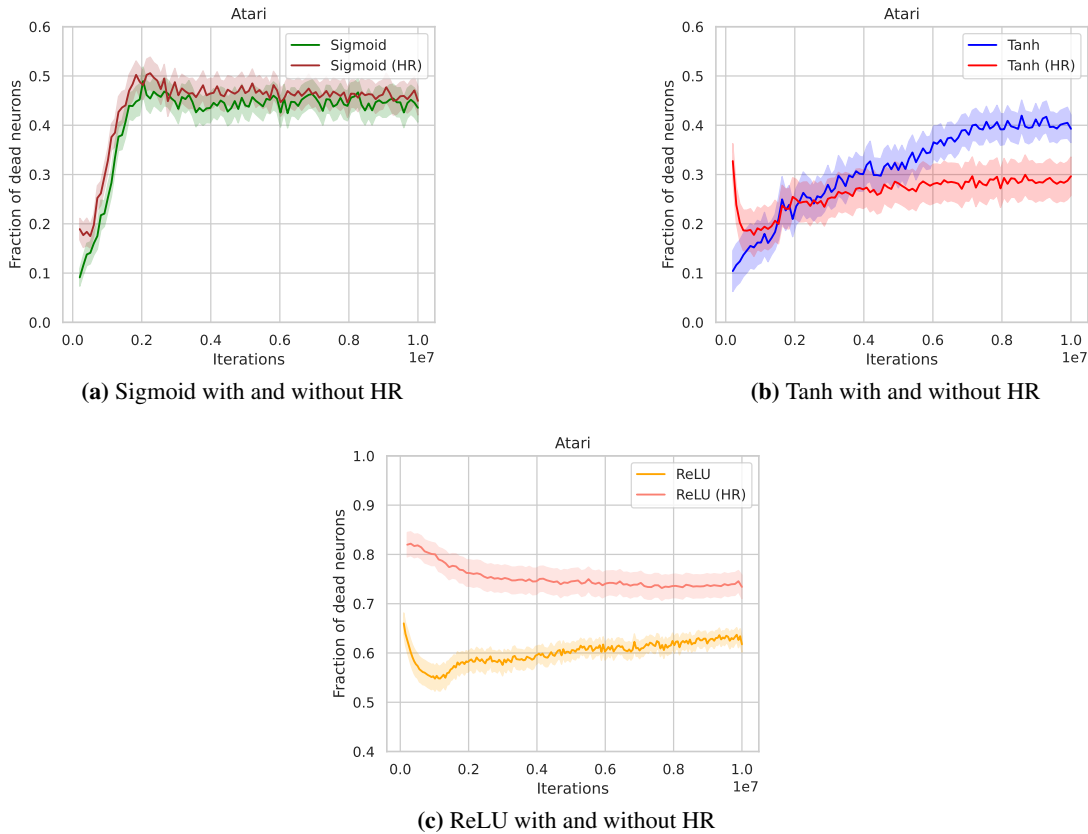


Figure 14: By evaluating the effect of an HR on dying neurons through the lens of probability theory, we predicted that only the hyperbolic tangent benefits in this metric. Specifically, only a hyperbolic tangent was speculated to have a decrease in dying neurons. Using an HR with sigmoid activations would have no notable difference, and for an HR with ReLU activations an increase in dead neurons was expected. This empirically validates our hypotheses in Section 4.

C.4. ReLU activated Hadamard representation

Additional Atari experiments are provided comparing a ReLU activation with and without an HR. The normalized scores, dying neurons and the effective rank during training can be seen in fig. 15.

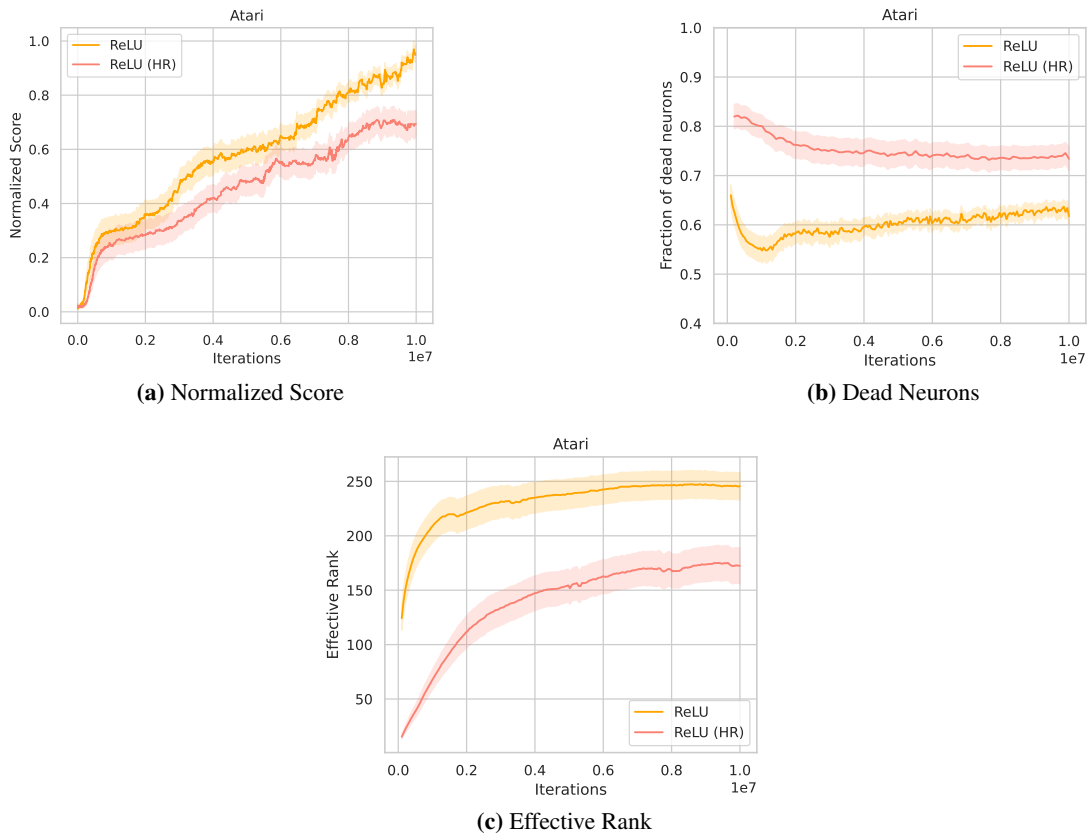


Figure 15: As a Rectified Linear Unit creates sparse representations, it does not benefit from using an HR, since the final representation will consist of the Hadamard product between two sparse representations. Therefore, a decrease in both performance and effective rank and an increase in dead neurons can be expected.

D. Atari

D.1. DQN & PPO Evaluation Details

For DQN and PPO, the Hadamard representation was applied to the final hidden layer of the Nature CNN. Furthermore, we have normalized performance with respect to the ReLU baseline on which the experiments were built (Huang et al., 2022). The minimum and maximum score of the ReLU baseline are taken for each environment, and the normalized score for each environment is calculated as follows:

$$\text{Normalized Score} = \frac{\text{Score} - \text{Min Score}}{\text{Max Score} - \text{Min Score}} \tag{8}$$

where *Score* refers to the raw performance score of the model being evaluated, *Min Score* is a single value representing the lowest score obtained by the ReLU baseline (usually equivalent to random policy or even slightly worse), and *Max Score* is a single value representing the highest score achieved by the ReLU baseline in the same environment. To average, we sum the normalized scores for every run and take the mean.

The more official Human-Normalized Score, as referenced in Mnih et al. (2015), is calculated similarly but using human and random performance benchmarks:

$$\text{Human-Normalized Score} = \frac{\text{Score} - \text{Random Score}}{\text{Human Score} - \text{Random Score}} \tag{9}$$

where *Human Score* and *Random Score* refer to the scores recorded by human players and random agents, respectively. Calculating our performance according to the Human-Normalized Score leads to the plot seen in Fig. 16. Due to taking a subset of the Atari domain in DQN and PPO, the VideoPinball environment is extremely dominant in the Human-Normalized Score calculation. For a more realistic comparison of the methods, we therefore decided to use baseline-normalized scores in the main paper.

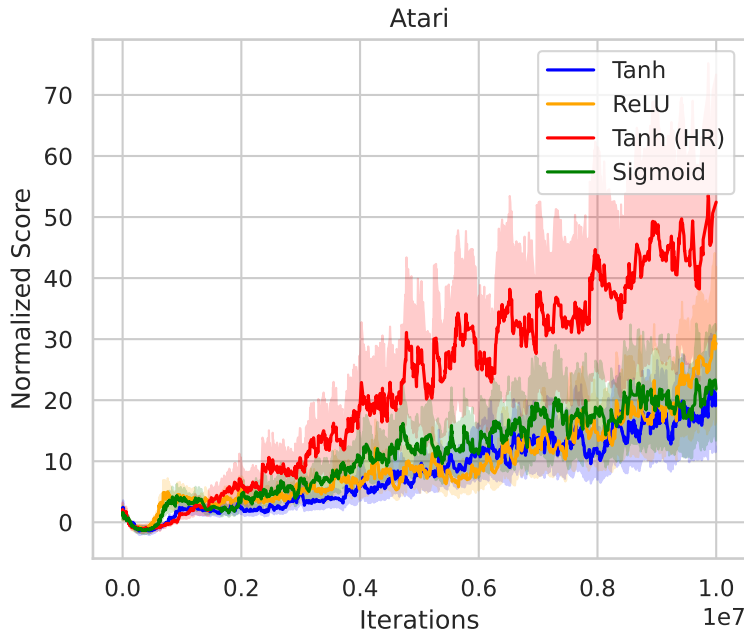


Figure 16: Human-Normalized performance (in multiples) with the standard deviation over the means in the Atari domain for 10M iterations (40M Frames).

D.2. Individual Environment Scores

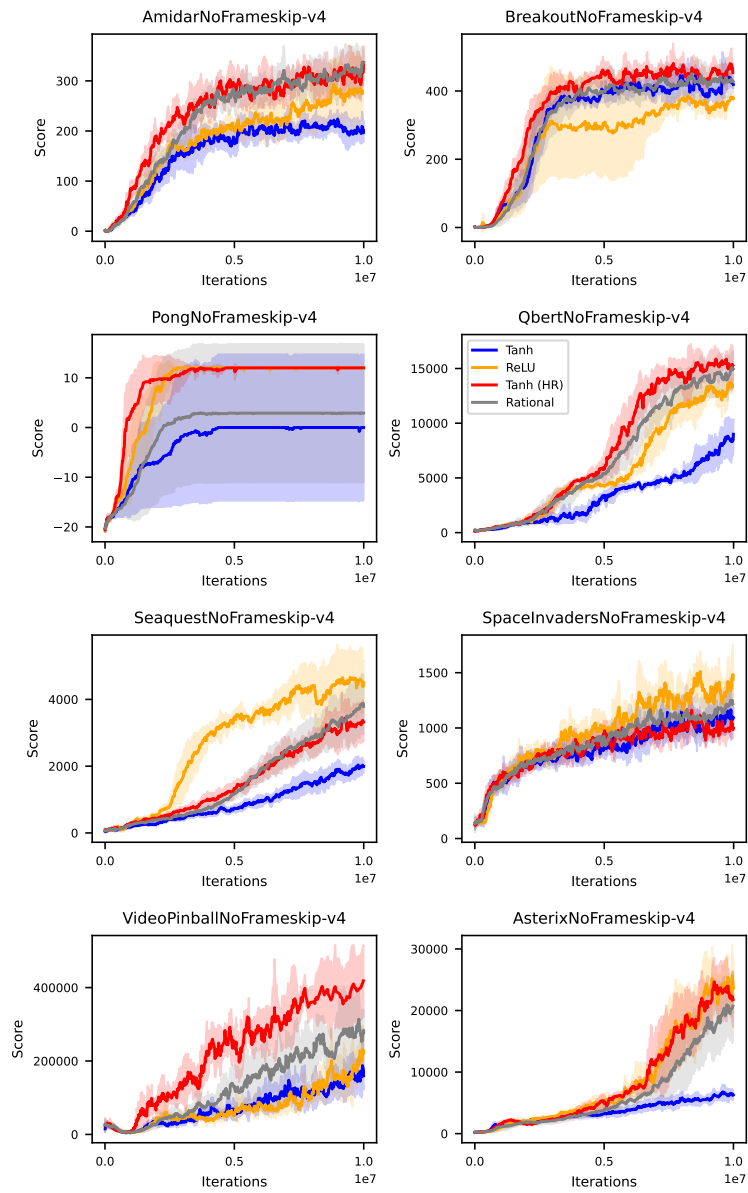


Figure 17: DQN Performance comparison on the individual Atari Environments. Plotted lines represent the mean taken over 5 seeds, with the standard deviations expressed as the shaded region.

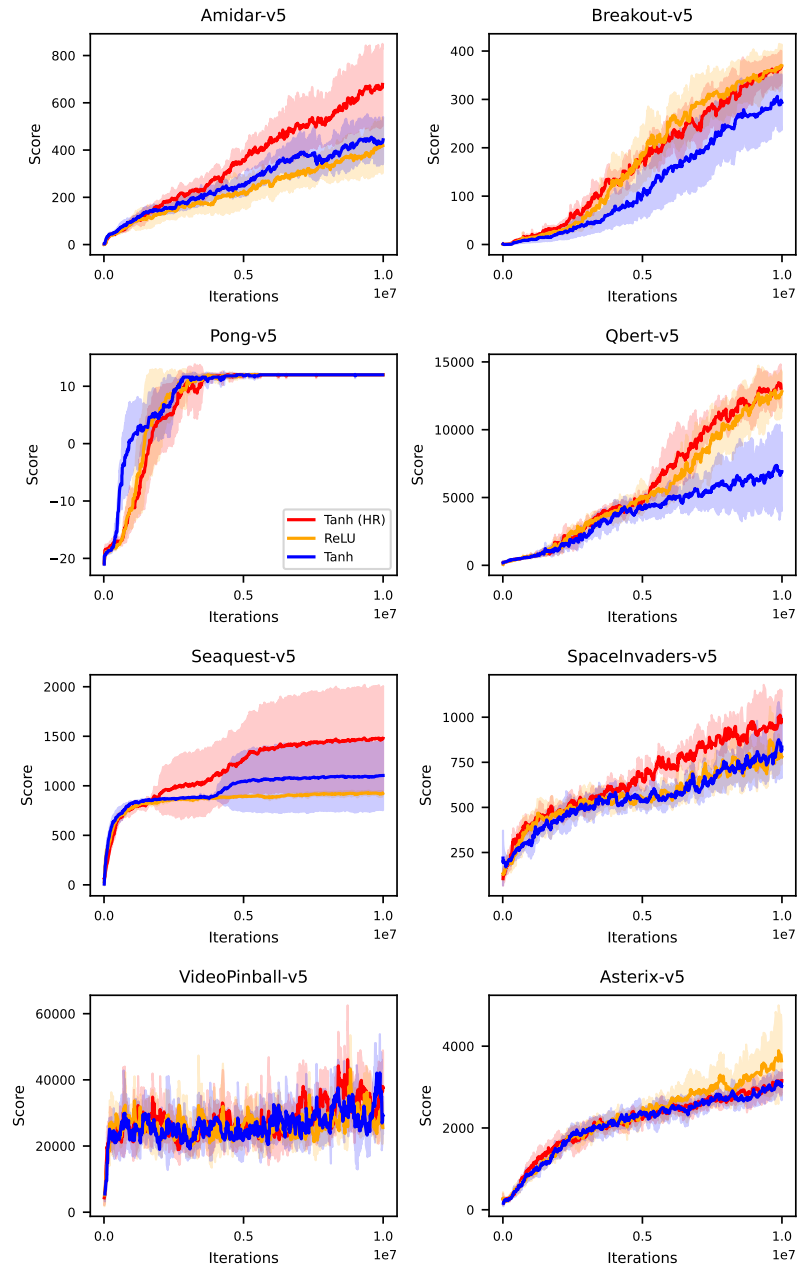


Figure 18: PPO Performance comparison on the individual Atari Environments. Plotted lines represent the mean taken over 5 seeds, with the standard deviations expressed as the shaded region.

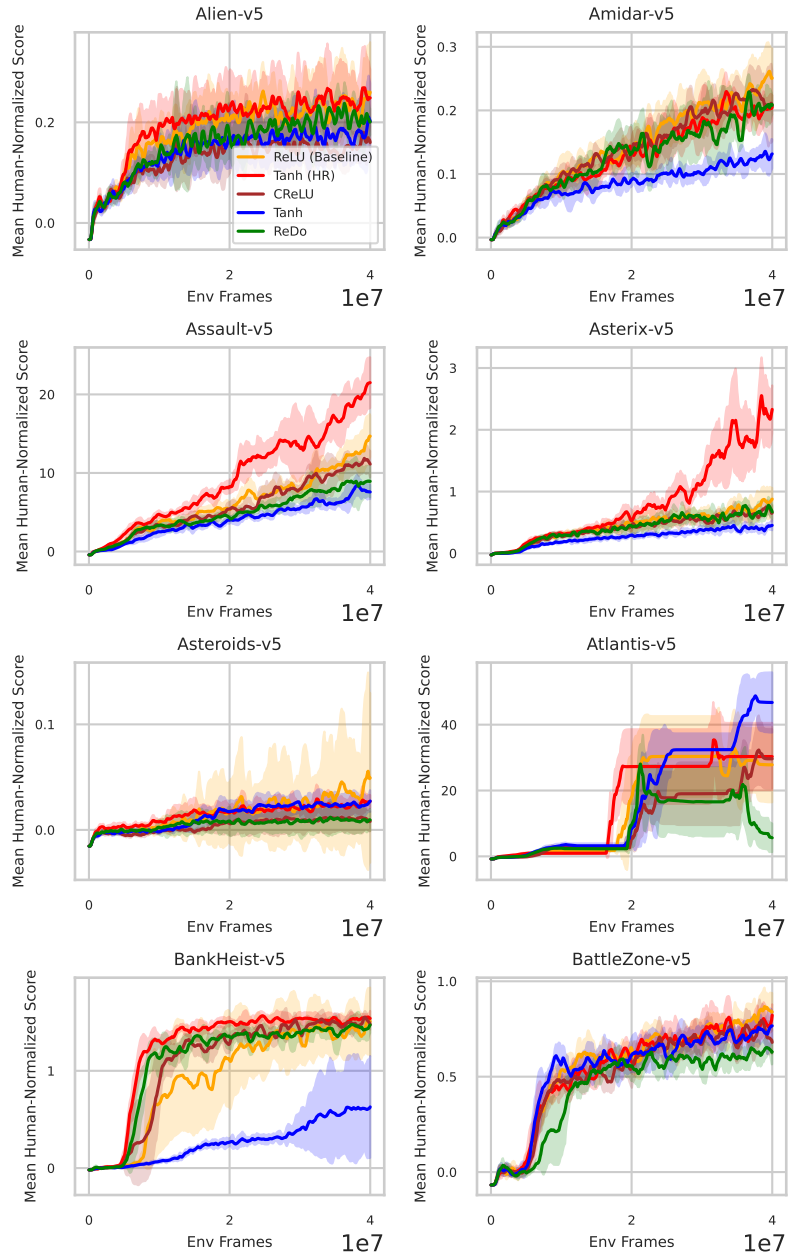


Figure 19: PQN Performance comparison on the individual Atari Environments. Labels represent encoder activations. Plotted lines represent the mean taken over 5 seeds, with the standard deviations expressed as the shaded region.

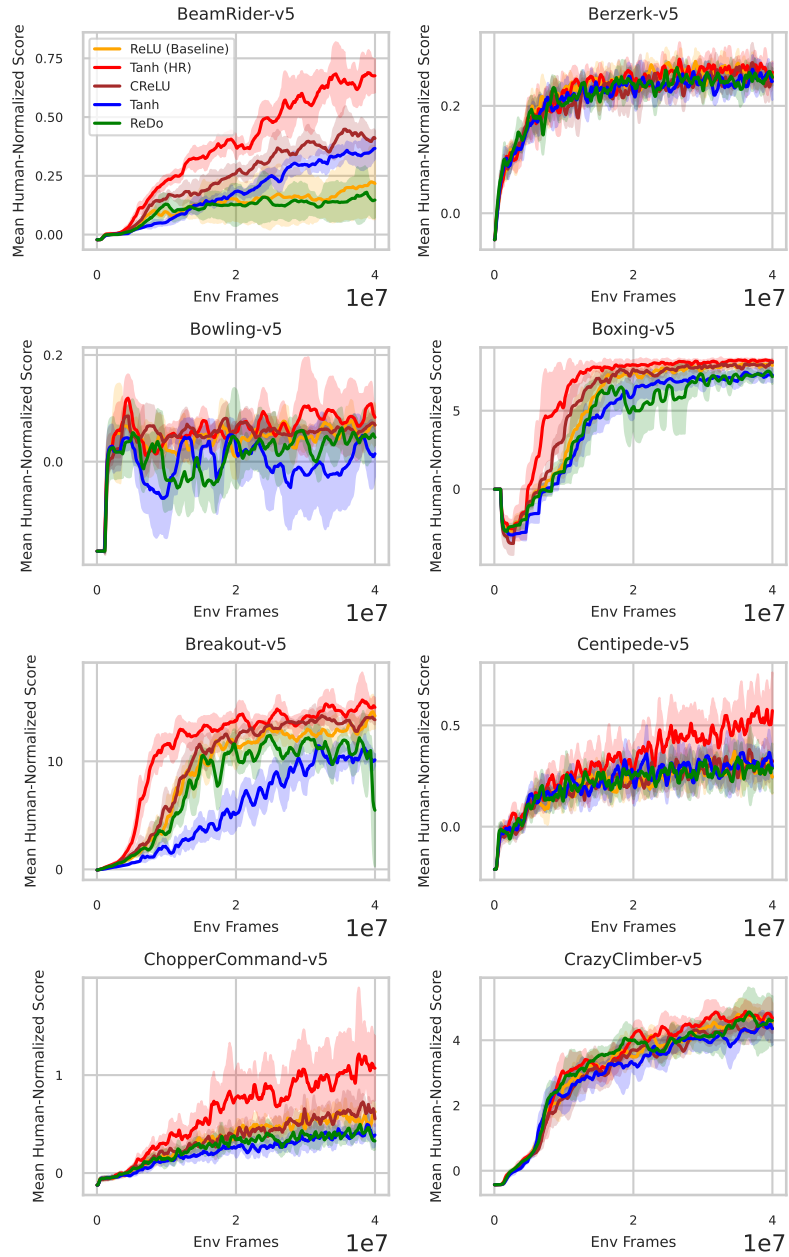


Figure 20: PQN Performance comparison on the individual Atari Environments. Labels represent encoder activations. Plotted lines represent the mean taken over 5 seeds, with the standard deviations expressed as the shaded region.

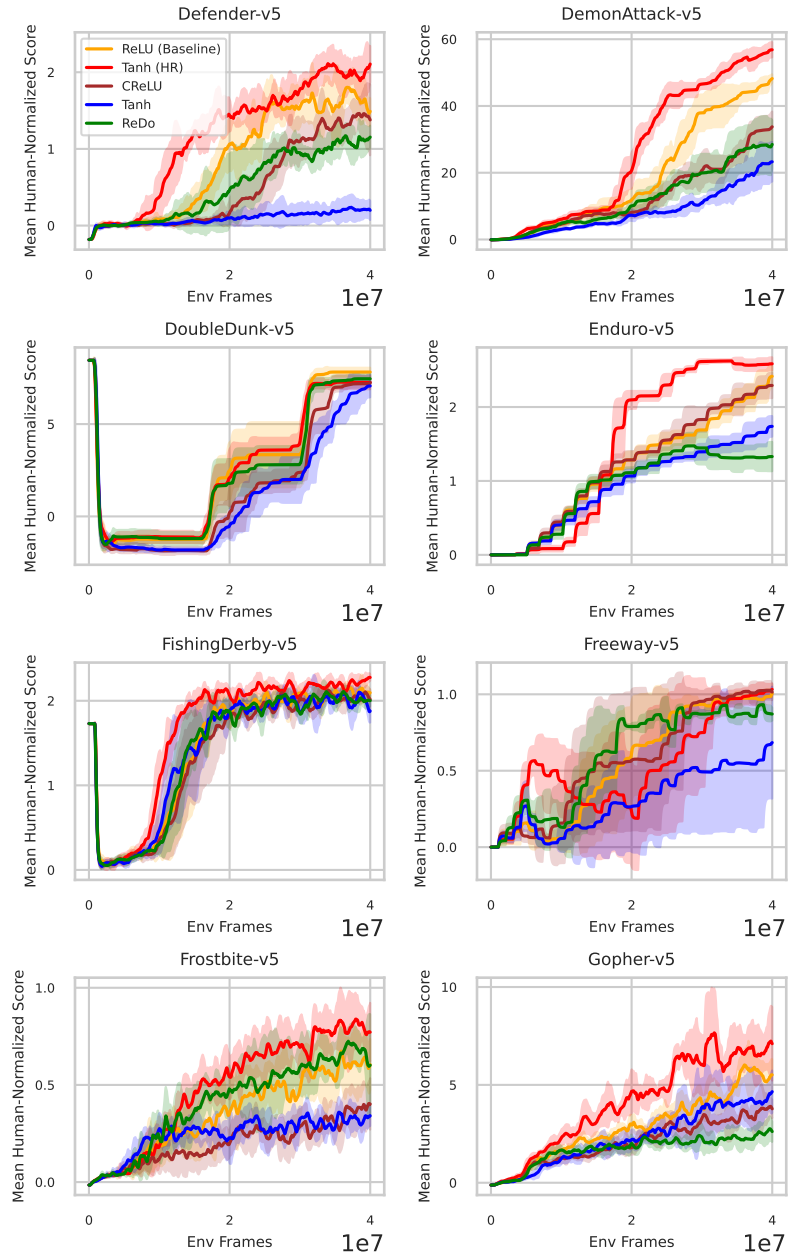


Figure 21: PQN Performance comparison on the individual Atari Environments. Labels represent encoder activations. Plotted lines represent the mean taken over 5 seeds, with the standard deviations expressed as the shaded region.

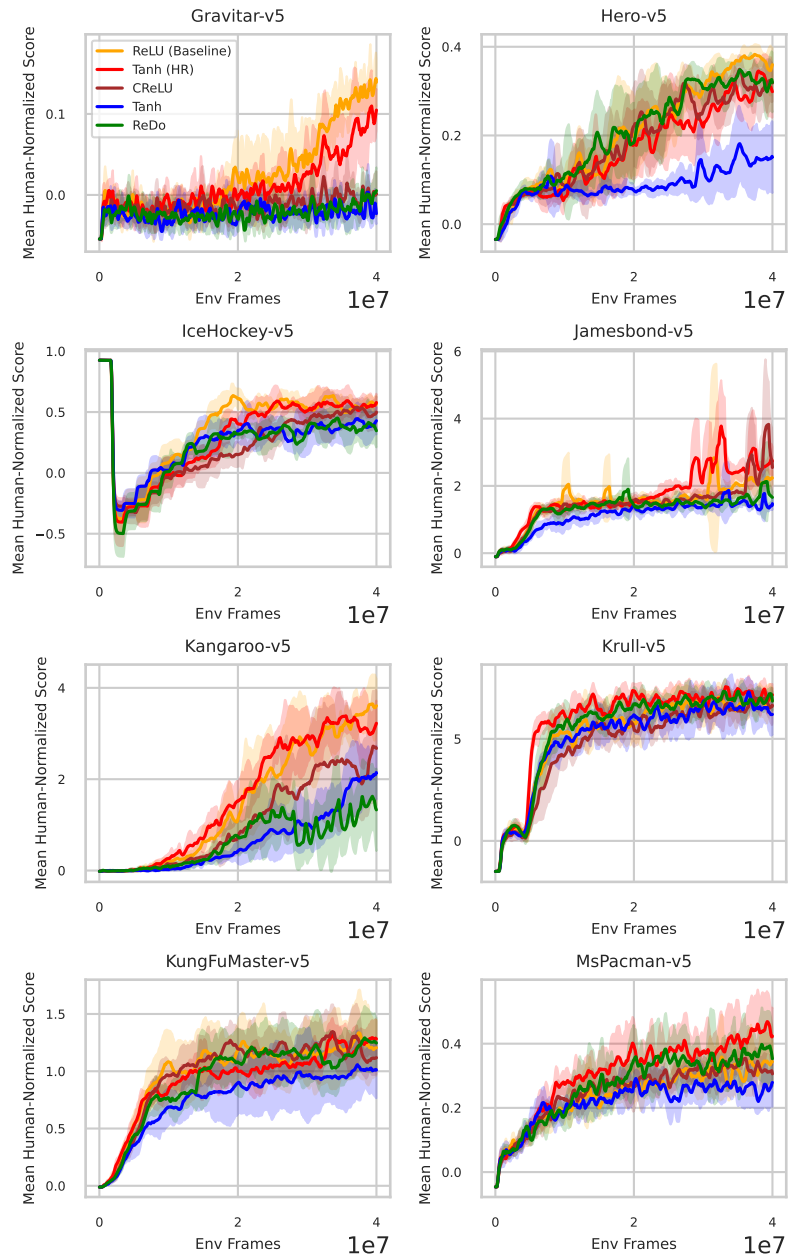


Figure 22: PQN Performance comparison on the individual Atari Environments. Labels represent encoder activations. Plotted lines represent the mean taken over 5 seeds, with the standard deviations expressed as the shaded region.

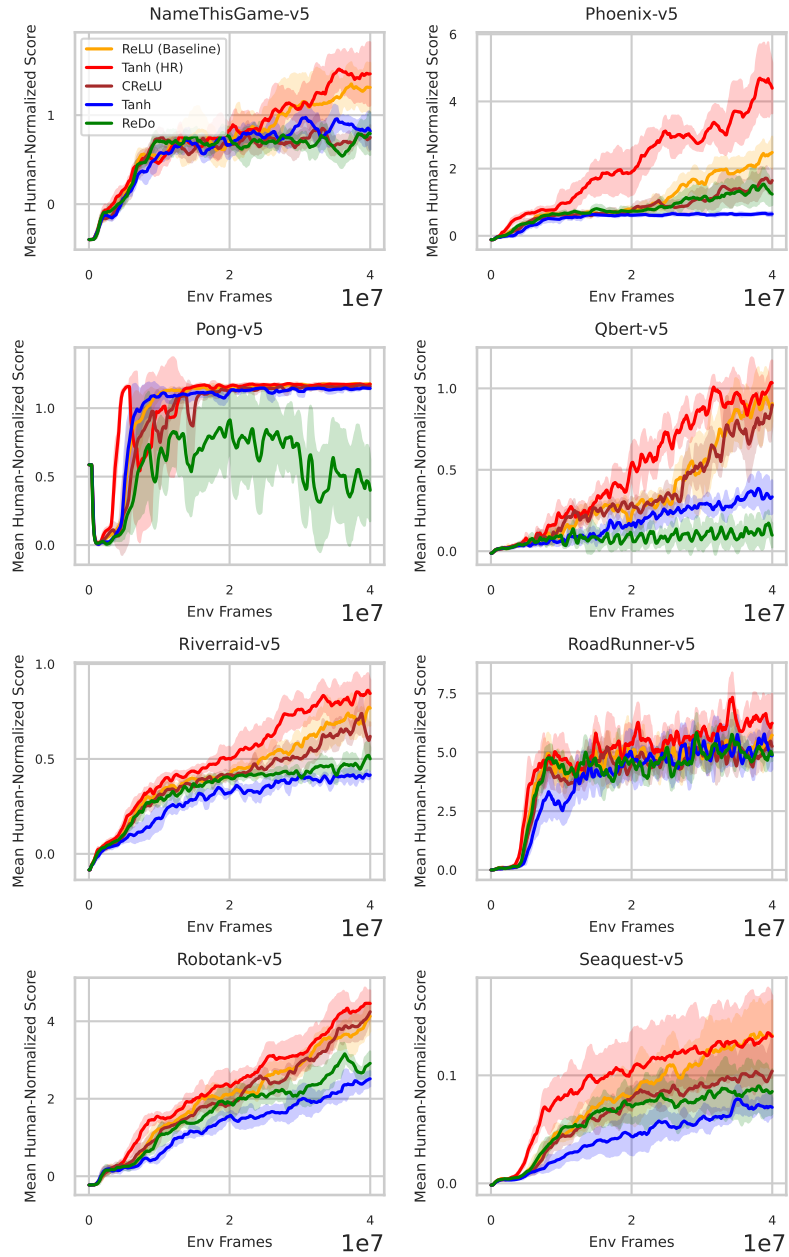


Figure 23: PQN Performance comparison on the individual Atari Environments. Labels represent encoder activations. Plotted lines represent the mean taken over 5 seeds, with the standard deviations expressed as the shaded region.

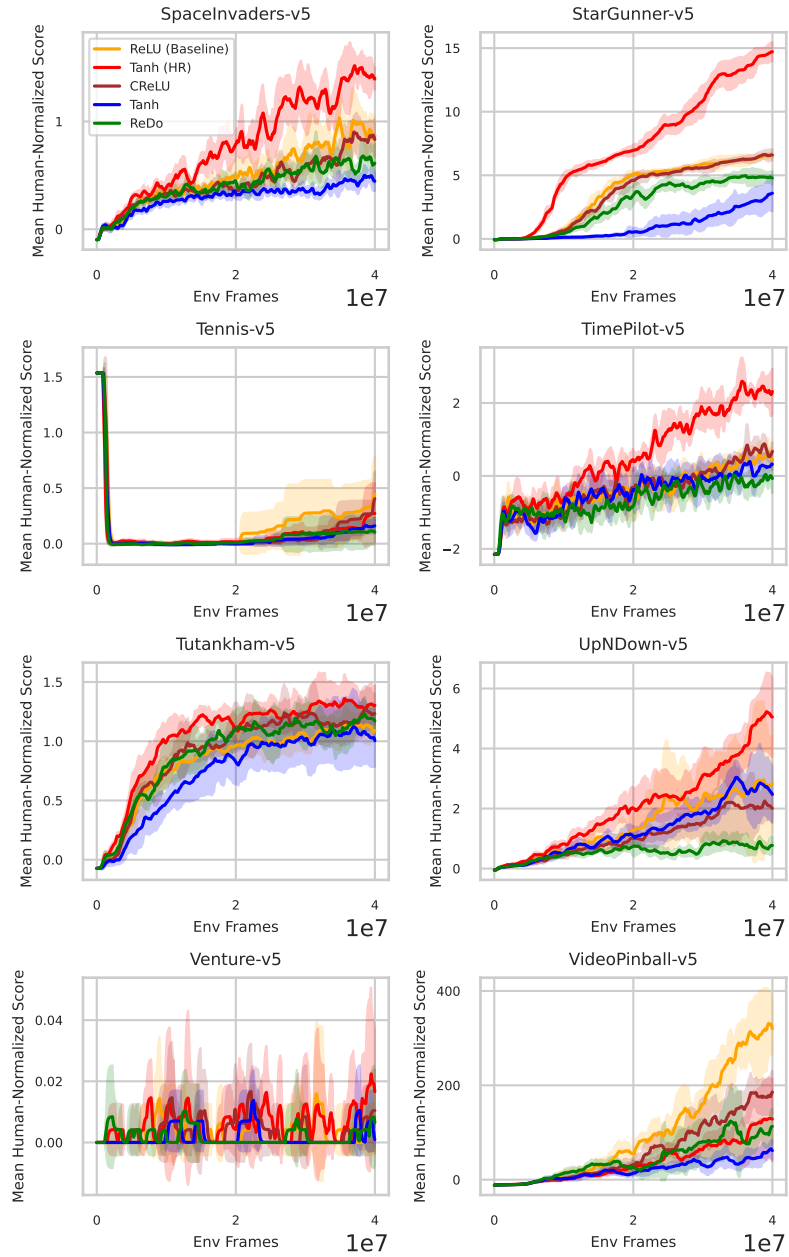


Figure 24: PQN Performance comparison on the individual Atari Environments. Labels represent encoder activations. Plotted lines represent the mean taken over 5 seeds, with the standard deviations expressed as the shaded region.

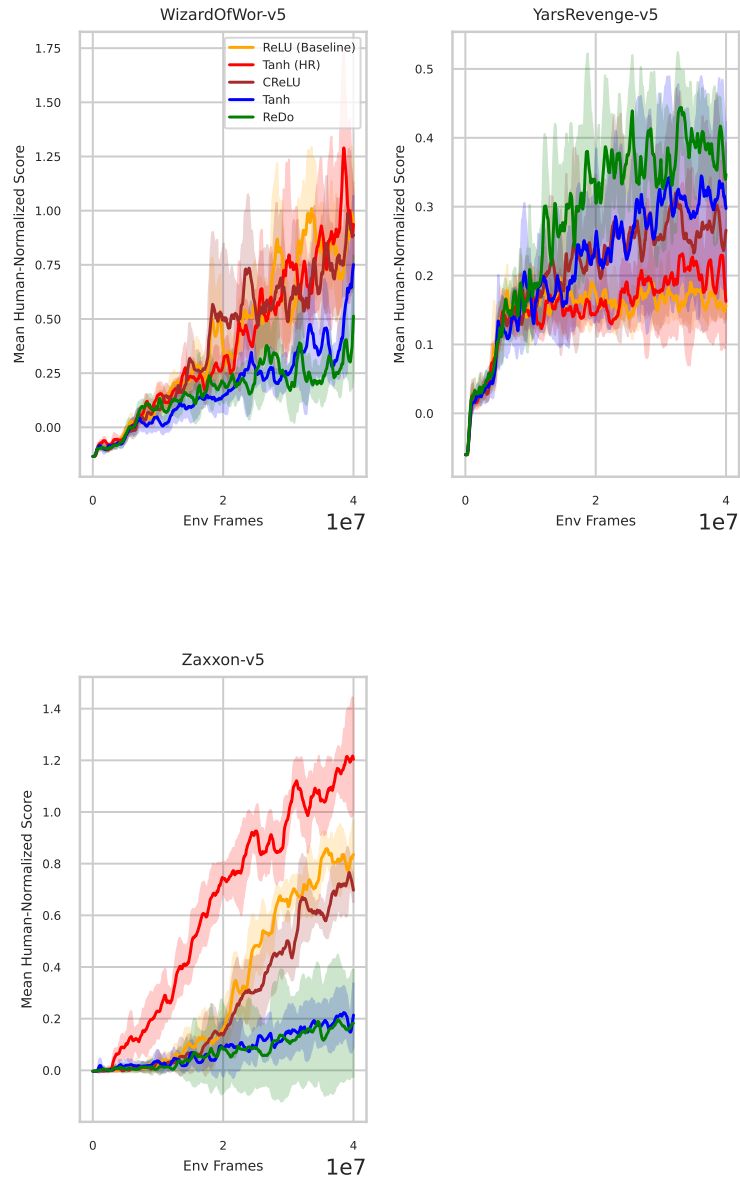


Figure 25: PQN Performance comparison on the individual Atari Environments. Labels represent encoder activations. Plotted lines represent the mean taken over 5 seeds, with the standard deviations expressed as the shaded region.